[32]K. Maki, Progr. Theoret. Phys. (Kyoto) Suppl. 211 (1968).
[33]A. Griffin, in *Superconductivity*, edited by P. R. Wallace (Gordon and Breach, New York, 1969), p. 577.
[34]E. Müller-Hartmann and J. Zittartz, Phys. Rev. Letters 26, 428 (1971).
[35]B. Coqblin and J. R. Schrieffer, Phys. Rev. 185, 847 (1969).
[36]B. Cornut and B. Coqblin (unpublished).
[37]A. S. Edelstein, L. R. Windmiller, J. B. Ketterson, G. H. Crabtree, and S. P. Bowen, Phys. Rev. Letters 26, 516 (1971).
[38]G. Riblet and K. Winzer, Solid State Commun. 9, 1663 (1971).
[39]M. B. Maple and K. S. Kim, Phys. Rev. Letters 23, 118 (1969).
[40]A. Griffin, Phys. Rev. Letters 15, 703 (1965).
[41]M. Fowler and K. Maki, Phys. Rev. 164, 484 (1967).
[42]A. S. Edelstein, Phys. Rev. Letters 19, 1184 (1967).
[43]A. S. Edelstein, Phys. Rev. 180, 505 (1969).
[44]J. Zittartz and E. Müller-Hartmann, Z. Physik 232, 11 (1970).
[45]M. Fowler and K. Maki, in Proceedings of Stanford International Conference on Superconductors, 1967 (unpublished); Phys. Rev. B 1, 181 (1970).
[46]B. T. Matthias, H. Suhl, and E. Corenzwit, Phys. Rev. Letters 1, 92 (1958).
[47]A. S. Edelstein, Phys. Letters 27A, 614 (1968).
[48]A. S. Edelstein, Phys. Rev. Letters 20, 1348 (1968).
[49]D. C. Golibersuch and A. J. Heeger, Phys. Rev. 182, 584 (1969).
[50]D. J. Scalapino, Phys. Rev. Letters 16, 937 (1966).
[51]P. M. Chaikin and M. A. Jensen, Solid State Commun. 8, 977 (1970).
[52]J. F. Tholence and R. Tournier, Phys. Rev. Letters 25, 867 (1970).

PHYSICAL REVIEW B VOLUME 6, NUMBER 3 1 AUGUST 1972

Quantum Interference Properties of Double Josephson Junctions

T. A. Fulton, L. N. Dunkleberger, and R. C. Dynes
Bell Telephone Laboratories, Murray Hill, New Jersey 07974
(Received 28 March 1972)

The dependence of the critical current I_c on magnetic field B in double Josephson tunnel junctions is discussed in a model which includes the dependence of junction critical currents, magnetic self-screening, and asymmetry. Account is taken both of static (zero-voltage) and dynamic (nonzero-voltage) behavior, the former controlling the over-all shape of $I_c(B)$ and the latter being important in nonadiabatic transitions between multiple states of the junction. The experimental $I_c(B)$ of double Sn-Sn tunnel junctions are interpreted in this model, and display effects of both static and dynamic origin.

I. INTRODUCTION

A well-known aspect of the Josephson effect[1-4] is quantum interference,[5-7] the oscillatory dependence on magnetic field B of the supercurrent flow and of the maximum supercurrent I_c that can be supported by single or multiple Josephson junctions. One of the simplest and most revealing geometries in which quantum interference can be observed is the double junction,[7-9] two individual weak-link junctions operated in parallel. Under certain assumptions, it is possible to interpret fully the $I_c(B)$ for this system,[10] taking exact account of the loop self-inductance and magnetic asymmetry and allowing a more general form for the supercurrent-phase relation of the junction than the usual sinusoid, first predicted for tunnel junctions by Josephson. The interpretation is thus sufficiently general to make contact with experiment and has been previously employed to interpret the $I_c(B)$ for Ta-Ta and Nb-Nb point-contact double junctions[10] and for Sn Anderson-Dayem bridges,[11,12] providing in these cases a simple relatively accurate determination of the supercurrent-phase relations. In this paper we describe effects occurring in the $I_c(B)$ of double junctions fabricated using superconductor-insulator-superconductor tunnel junctions,[7] the junctions originally discussed by Josephson.[1] Interpretation of the observed behavior requires that the dynamical aspects of the supercurrent flow in the double junction be taken into account, and we extend our previous treatment[10] of the static aspects of the supercurrent flow to include these.

Section II analyzes the properties of the steady-state supercurrent flow and describes a mechanical analog (the double pendulum). Section III discusses the dynamical effects. Section IV describes and interprets experiments on the $I_c(B)$ of double Josephson tunnel junctions.

II. SUPERCURRENT FLOW IN SMALL DOUBLE JUNCTIONS

In this section we review our approach to the analysis of the double junctions. We also describe an exact mechanical analog (the double pendulum) whose behavior simplifies the qualitative understanding of double junction behavior.

A. Analysis

Consider two bulk superconductors whose dimensions are large compared to the penetration depth and which are connected at two points by weak-link junctions forming a parallel circuit [Fig. 1(a)]. We assume that the junctions are small and that the magnetic fields to which they are subjected (from external sources or their own currents) are weak enough that the magnetic flux passing through the barrier and the adjacent penetration depths of the superconductors is much less than a flux quantum $\Phi_0 = h/2e = 2.07 \times 10^{-15}$ Wb. Then the supercurrent I passing through a single junction from one superconductor to the other can be expressed as a function of ϕ, the gauge-invariant phase difference between the order parameters of the bulk superconductors on either side of the barrier. These functions, $I_1(\phi_1)$ and $I_2(\phi_2)$ for junction Nos. 1 and 2, respectively, are taken to be formally periodic in ϕ modulo 2π, but are otherwise unrestricted. In particular they may be nonsinusoidal and are not necessarily smooth, continuous, or even single valued.

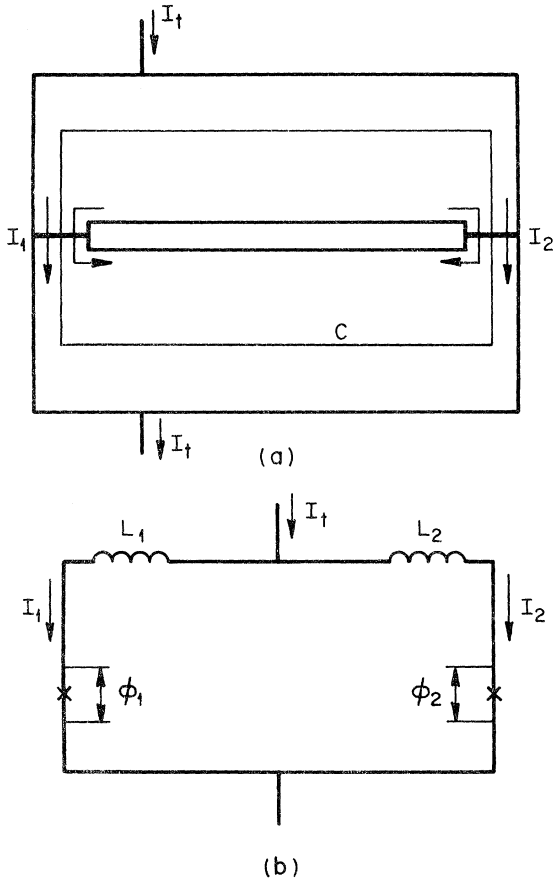

FIG. 1. (a) Schematic double weak-link junction. (b) Equivalent circuit of the double junction.

The net transport supercurrent I_t carried by the junction is

$$I_t = I_1(\phi_1) + I_2(\phi_2) \ . \tag{1}$$

Additionally there is the usual constraint[2] on the difference between ϕ_1 and ϕ_2, namely,

$$\phi_2 - \phi_1 = 2\pi\Phi/\Phi_0 \ , \tag{2}$$

where Φ is the total magnetic flux linking a contour C which [Fig. 1(a)] passes through the two weak links and elsewhere through the bulk superconductors at a depth much greater than the penetration depth. By the previous assumptions any change in the position at which the contour passes through the junctions changes Φ by an amount negligible compared to Φ_0. The effect of flux in the junctions from external sources could be dealt with by assuming I_{c1} and I_{c2} to be B dependent, giving the usual diffraction background of the interference pattern of $I_c(B)$. Addition of self-fields within the junctions,[3,13,14] a further complication, will not be considered.

The magnetic flux Φ is the sum of two parts. The first, denoted Φ_x, comes from the applied B field modified by the diamagnetic screening of the bulk superconductors. The second, denoted Φ_s, is due to the magnetic fields set up by the flow of I_1 and I_2. If Φ_s is negligible the phase difference $\phi_2 - \phi_1$ is fixed for fixed B, and (1) and (2) reduce to

$$I_t = I_1(\phi_1) + I_2(\phi_1 + 2\pi\Phi_x/\Phi_0) \ . \tag{3}$$

For fixed I_t it is straightforward to find the value of ϕ_1 satisfying (3), and hence the separate values of I_1 and I_2. For sinusoidal $I(\phi)$ this can be done analytically. More generally a solution can be found graphically for any $I(\phi)$ by simply adding I_1 and I_2 displaced in phase by $2\pi\Phi_x/\Phi_0$ and finding the points at which the sum equals I_t. If Φ_s is not negligible then (1) and (2) are coupled and their solution becomes ostensibly more difficult. Numerical solutions in a few particular cases[15] have previously been given.

From our assumption of small junctions it follows that essentially all of the contribution to Φ_s from I_1 and I_2 comes from the flow of these currents in the penetration depths of the bulk materials. The junctions act as point current sources supplying the surface currents of the bulk materials, and the surface current density and its resultant magnetic field are linear superpositions of the currents and fields caused by I_1 and I_2 acting separately (as well as, of course, the surface current flow induced by the exterior magnetic field). Hence we may write Φ_s as a linear expression

$$\Phi_s = L_1 I_1 - L_2 I_2 \ , \tag{4}$$

where L_1 and L_2 are coefficients having the units

of inductance and the signs are taken so that L_1 and L_2 are positive in most geometries. The sum of L_1 and L_2 is L, the self-inductance of the double junction loop, but L_1 and L_2 separately usually cannot be interpreted as individually describing the inductance of separate portions of the loop. Nonetheless it is often useful to employ the equivalent circuit of Fig. 1(b) in which L_1 and L_2 are treated as separate lumped inductances. We shall assume henceforth that L_1 and L_2 are non-negative, considering the importance of negative L briefly in Appendix A.

With (4), the constraint (2) can be written as

$$\phi_2 - \phi_1 = 2\pi\Phi_x/\Phi_0 + 2\pi L_1 I_1/\Phi_0 - 2\pi L_2 I_2/\Phi_0 . \quad (5)$$

This constraint is much simplified by using a new set of variables θ_1, θ_2, and θ_x defined by

$$\theta_1 = \phi_1 + 2\pi L_1 I_1(\phi_1)/\Phi_0 , \quad (6)$$

$$\theta_2 = \phi_2 + 2\pi L_2 I_2(\phi_2)/\Phi_0 , \quad (7)$$

$$\theta_x = 2\pi\Phi_x/\Phi_0 . \quad (8)$$

Note that θ_1 and θ_2 depend only on the value of ϕ_1 and ϕ_2, respectively, while θ_x is a normalized measure of B. Expressed in these terms (5) becomes

$$\theta_2 - \theta_1 = \theta_x . \quad (9)$$

One may also use θ_1 and θ_2 rather than ϕ_1 and ϕ_2 as the independent variables determining I_1 and I_2, denoting the function $I_1(\phi_1(\theta_1))$ by $I_1(\theta_1)$ and similarly $I_2(\phi_2(\theta_2))$ by $I_2(\theta_2)$. Equation (1) then becomes

$$I_t = I_1(\theta_1) + I_2(\theta_2) . \quad (10)$$

Equations (9) and (10) replace Eqs. (1) and (2) as the basic equations of the problem and can immediately be combined to give

$$I_t = I_1(\theta_1) + I_2(\theta_1 + \theta_x) . \quad (11)$$

[For brevity we will subsequently denote $I_1(\theta_1) + I_2(\theta_1 + \theta_x)$ by $I_s(\theta_1, \theta_x)$.] This equation has precisely the same form as (3) and the same graphical approach to determining the $I_c(B)$ and other features of the supercurrent flow may be used. In effect the change of variables replaces the problem involving $L \neq 0$ by an equivalent $L = 0$ problem having current-phase relations with a modified shape.

Figure 2 gives two examples of the relation between ϕ and θ and the construction of the $I(\theta)$. In Figs. 2(a) and 2(b), we take $I_1(\phi_1) = I_{c1}\sin\phi_1$ and $2\pi L_1 I_{c1}/\Phi_0 = 0.45$. The $I_1(\phi_1)$ and also a straight line given by $I_1 = -(\Phi_0/2\pi L_1)\phi_1$ are plotted in Fig. 2(a). For each point P of $I_1(\phi_1)$ there is a corresponding value $\theta_1(P)$ whose magnitude is the horizontal distance between that point and the diagonal line. The function $I_1(\theta_1)$ is generated by taking these corresponding values of $I_1(P)$ and $\theta_1(P)$ for

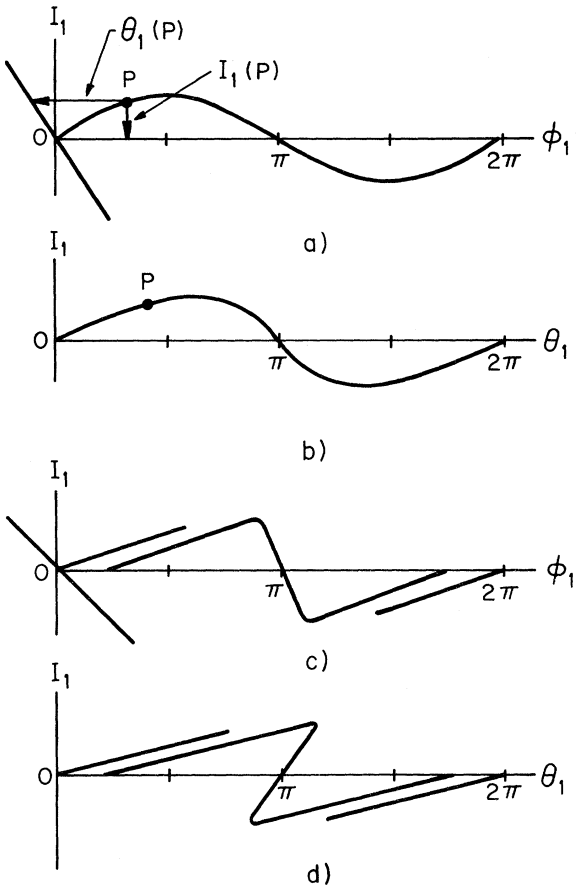

FIG. 2. Construction of $I(\theta)$ from $I(\phi)$. (a) and (b) Sinusoidal $I(\phi)$. (c) and (d) Nonsinusoidal, multivalued $I(\phi)$.

all points P on the curve. Figure 2(b) plots $I_1(\theta_1)$ for the case of Fig. 2(a) and illustrates the general point that $I_1(\theta_1)$ has the appearance of a skewed $I_1(\phi_1)$, rising more slowly and descending more steeply than the latter. Figure 2(c) shows a more complicated example, taking a discontinuous multivalued $I_1(\phi_1)$. We have taken $2\pi L_1 I_{c1}/\Phi_0 = 0.72$, where I_{c1} is the maximum value of I_1. The same procedure for constructing $I_1(\theta_1)$ applies, and this function is shown in Fig. 2(d). In this case the skewing is sufficient to create reentrant portions in $I_1(\theta_1)$, corresponding to all parts of $I_1(\phi_1)$ having a steep enough negative slope, i.e., $dI_1/d\phi_1 < -\Phi_0/2\pi L_1$.

Using Eq. (11) one may obtain a complete picture of the supercurrent flow in a double junction given $I_1(\phi_1)$, $I_2(\phi_2)$, L_1, and L_2. We shall discuss three examples which illustrate most of the phenomena that occur. We emphasize the $I_c(B)$, or $I_c(\theta_x)$, as this is what we measure experimentally, and we restrict ourselves to $I(\phi) = I_c\sin\phi$ although many of

the qualitative results will obviously occur in nonsinusoidal cases as well. To avoid obscuring the results we set forth the manipulations of Eqs. (1)–(11) involved in the less obvious points in Appendix A. Certain comments involving the stability of some solutions draw on results to be derived in Sec. III.

A convenient set of parameters are $\alpha_1 = 2\pi L_1 I_{c1}/\Phi_0$, $\alpha_2 = 2\pi L_2 I_{c2}/\Phi_0$, I_{c2}/I_{c1}, and I_{c1}. We shall suppose that $I_{c2} \leqq I_{c1}$. Note that for fixed α_1, α_2, and I_{c2}/I_{c1} the currents for a given θ_x scale with I_{c1}, so that qualitative changes in, say, $I_c(\theta_x)$ result only from changes in the first three parameters. Although all three variables affect the shape of $I_c(\theta_x)$ it turns out (Appendix A) that I_{c2}/I_{c1} and the parameter which we shall call α, where $\alpha = 2\pi L I_{c2}/\Phi_0 = \alpha_2 + \alpha_1(I_{c2}/I_{c1})$, are of particular importance in determining the major qualitative features of $I_c(\theta_x)$. In Fig. 3, we show the various regimes of α and I_{c2}/I_{c1} in which qualitatively dissimilar behavior is found. These regimes, which we have labeled A, C, and B, are set off by the heavy solid lines and roughly correspond to regimes of increasing importance of the self-fields. Our three examples are taken at the points indicated by the crosses. The determination of the boundaries of A, B, and C will be described subsequently.

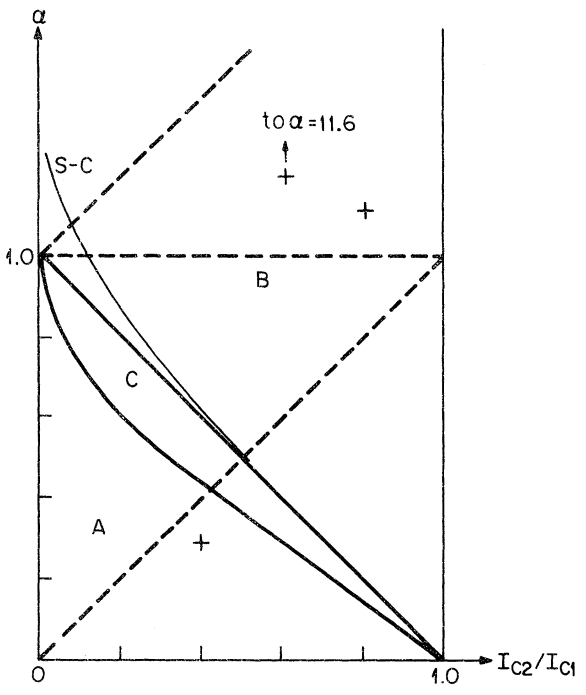

FIG. 3. A, B, and C are regions of qualitatively different behavior of $I_c(\theta_x)$ in its dependence on I_{c2}/I_{c1} and $\alpha = 2\pi L I_{c2}/\Phi_0$. The dashed lines set off differing regions of single-valued and multivalued $I_1(\theta_1)$ and $I_2(\theta_2)$. The line S-C indicates the transition between smooth and cusplike minima of $I_c(\theta_x)$. The crosses indicate the values of α and I_{c2}/I_{c1} for the three examples of the text.

Note that if $\alpha \leq 1$ then $\alpha_2 \leq 1$ and $I_2(\theta_2)$ is single valued, while if $\alpha/(I_{c2}/I_{c1}) < 1$ then $\alpha_1 \leq 1$ and both $I_1(\theta_1)$ and $I_2(\theta_2)$ are single valued. Both $I_1(\theta_1)$ and $I_2(\theta_2)$ may still be single valued for any α and I_{c2}/I_{c1} obeying $\alpha < 1 + (I_{c2}/I_{c1})$. These regions of single and double valuedness are indicated by the dashed lines of Fig. 3, and do not coincide with the boundaries of A, B, or C. The significance of the light line denoted S-C will be described in the second example.

First example. Suppose that α_1 and α_2 are small corresponding to region A of Fig. 3. The limit $\alpha_1 = \alpha_2 = 0$ is the familiar $L = 0$ problem, and gives $I_c(\theta_x) = (I_{c1}^2 + I_{c2}^2 + 2I_{c1}I_{c2}\cos\theta_x)^{1/2}$. For $\alpha_1 \ll 1$ and $\alpha_2 \ll 1$ the deviation from the $L = 0$ result is small. Figure 4 shows an example of the graphical procedure for solving Eq. (11) in this particular limit. Here we construct $I_1(\theta_1)$ and $I_2(\theta_2)$ from sinusoids using $I_{c1} = 1.0$, $I_{c2} = 0.4$, $\alpha_1 = 0.1$, and $\alpha_2 = 0.25$, so that $I_{c2}/I_{c1} = 0.4$ and $\alpha = 0.29$. In Fig. 4(a), we show $I_1(\theta_1)$, $I_2(\theta_2)$, and $I_s(\theta_1, \theta_x)$ for $\theta_x = 0$ and in Fig. 4(b) for $\theta_x = \pi$. Note that the maxima of $I_1(\theta_1)$ and $I_2(\theta_2)$ occur at $\theta_1 = \frac{1}{2}\pi + \alpha_1$ and $\theta_2 = \frac{1}{2}\pi + \alpha_2$, respectively, while the maximum and minimum slopes of $I_1(\theta_1)$ at $\theta = 0$ and $\theta_1 = \pi$ are $dI_1/d\theta_1 = \pm I_{c1}/(1 \pm \alpha_1)$ and correspondingly for $I_2(\theta_2)$ the slopes at $\theta_2 = 0$ and $\theta_2 = \pi$ are $dI_2/d\theta_2 = \pm I_{c2}/(1 \pm \alpha_2)$. In solving (11) graphically, for a given $I_t = \bar{I}_t$ we find that θ_1 for which $I_s(\theta_1, \theta_x) = \bar{I}_t$. The intersection of the dotted line in Fig. 4(a) with $I_s(\theta_1, \theta_x)$ gives these θ_1. In all cases for most I_t there are at least two θ_1 satisfying $I_s(\theta_1, \theta_x) = I_t$, e.g., P_1 and P_2 in Fig. 4(a). Of these only those corresponding to the portion of $I_s(\theta_1, \theta_x)$ having positive slope, such as P_1, represent a dynamically stable situation (see Sec. III). Having found the θ_1, call it $\bar{\theta}_1$ for $\bar{I}_t$, the junction currents are given by $I_1(\bar{\theta}_1)$ and $I_2(\bar{\theta}_1 + \theta_x)$, the magnetic self-flux by $L_1 I_1(\bar{\theta}_1) - L_2 I_2(\bar{\theta}_1 + \theta_x)$, and so on.

The positive (negative) critical current I_{c+} (I_{c-}) is the maximum (minimum) value of $I_s(\theta_1, \theta_x)$ at each θ_x, a plot of $I_{c+}(\theta_x)$ derived in this manner being shown in Fig. 4(c). The $I_{c-}(\theta_x)$ has a shape similar to that of $I_{c+}(\theta_x)$, the two being related by the time-reversal requirement $I_{c+}(\theta_x) = -I_{c-}(-\theta_x)$. As for the $L = 0$ case this $I_{c+}(\theta_x)$ is a smoothly varying periodic function and is typical of type-A situations. Some salient features are these: (i) The maximum of $I_{c+}(\theta_x)$ is $(I_{c1} + I_{c2})$ and occurs when the maxima of $I_1(\theta_1)$ and $I_2(\theta_1 + \theta_x)$ are aligned, at $\theta_x = \alpha_2 - \alpha_1$. This occurs at $\theta_x = 0$ ($B = 0$) only if $\alpha_1 = \alpha_2$. It turns out (see Appendix A) that the minimum of I_{c+} is $(I_{c1} - I_{c2})$ and occurs when the maximum of $I_1(\theta_1)$ is aligned with the minimum of $I_2(\theta_1 + \theta_x)$, at $\theta_x = \pi - (\alpha_2 + \alpha_1)$. (ii) Since the angular

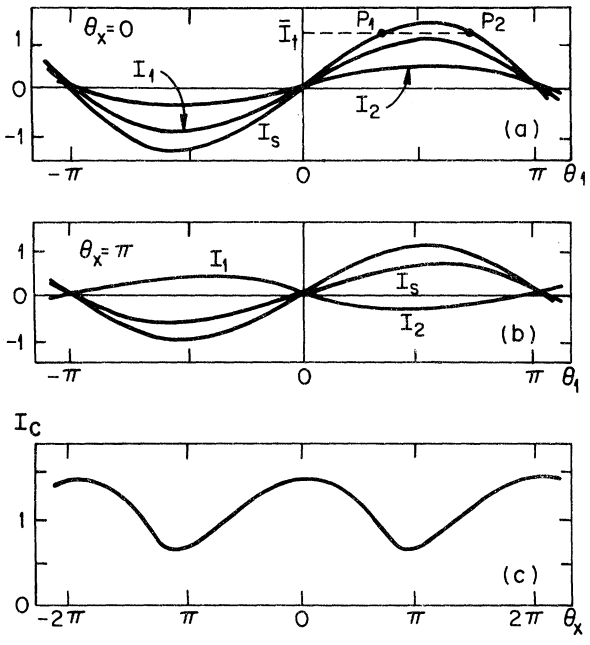

FIG. 4. (a) $I_1(\theta_1)$, $I_2(\theta_1+\theta_x)$, and $I_s(\theta_1, \theta_x)$ for $I_{c1}=1$, $I_{c2}=0.4$, $\alpha_1=0.1$, $\alpha_2=0.25$, and $\theta_x=0$. Points P_1 and P_2 are two solutions to $I_s(\theta_1, 0)=\bar{I}_t$. (b) Same except $\theta_x=\pi$. (c) $I_c(\theta_x)$ for these parameters.

separation between the maximum and minimum of I_{c+} in the direction of increasing θ_x is $\pi-2\alpha_2$ and in the direction of decreasing θ_x is $\pi+2\alpha_2$, $I_c(\theta_x)$ is always asymmetric in the regime A if $\alpha_2\neq 0$. This asymmetry persists in B and C regimes with the single exception of the case $\alpha_1=\alpha_2$ and $I_{c2}/I_{c1}=1$. (iii) From (i) and (ii) it follows that the positions and magnitudes of I_{c+} at its maximum and minimum determine the parameters α_1, α_2, I_{c2}/I_{c1}, and I_{c1} for sinusoidal $I_s(\phi)$. Experimental examples of this will be given in Sec. IV. (iv) The maximum and minimum first derivative or slope of $I_{c+}(\theta_x)$ is $dI_{c+}/d\theta_x=\pm I_{c2}/(1\pm\alpha_2)$. (v) The shape of $I_c(\theta_x)$ in the A regime is uniquely related to $I_2(\theta_2)$ and can be used to generate it (see Appendix A). In the limit $\alpha+I_{c2}/I_{c1}\ll 1$, $I_c(\theta_x)$ has exactly the same shape as $I_2(\theta_2)$ [which in turn for $\alpha_2\ll 1$ tends to $I_2(\phi_2)$ in its shape]. If this inequality is not strongly obeyed the shape of $I_c(\theta_x)$ becomes a distorted version of $I_2(\theta_2)$ with the maxima somewhat broadened and the minima somewhat pinched. There is, however, a procedure (Appendix A) for removing this distortion and recovering $I_2(\theta_2)$. Thus a double junction having $\alpha\ll 1$ provides a direct means of measuring $I(\phi)$ in weak links for which the shape is not known.[10,12]

Second example. For values of I_{c2}/I_{c1} and α lying outside regime A a new situation occurs, illustrated by the example in Fig. 5. Here the parameters are $I_{c1}=1.0$, $I_{c2}=0.8$, $\alpha_1=0.4$, and $\alpha_2=0.8$ so that $I_{c2}/I_{c1}=0.8$ and $\alpha=1.12$, a case in regime B of Fig. 3. Figures 5(a)–5(c) show $I_1(\theta_1)$, $I_2(\theta_2)$, and $I_s(\theta_1, \theta_x)$ for $\theta_x=0$, $\frac{3}{4}\pi$, and π. The new element is that for some θ_x the function $I_s(\theta_1, \theta_x)$ develops a double maximum and minimum as in Fig. 5(b). This situation occurs in regime B because the condition $I_{c1}/(1+\alpha_1)<I_{c2}/(1-\alpha_2)$ or $I_{c2}/I_{c1}+\alpha\geq 1$ holds there, the boundary of B being $I_{c2}/I_{c1}+\alpha=1$. Thus at $\theta_x=\pi$ the slope $dI_s(\theta_1, \theta_x)/d\theta_1$ is negative at both $\theta_1=0$ [at which $dI_s(\theta_1, \theta_x)/d\theta_1=I_{c1}/(1+\alpha_1)-I_{c2}/(1-\alpha_2)$] and at $\theta_1=\pi$ [at which $dI_s(\theta_1, \theta_x)=-I_{c1}/(1-\alpha_1)+I_{c2}/(1+\alpha_2)$]. Hence $I_s(\theta_1, \theta_x)$ must possess two maxima and minima between $\theta_1=0$ and $\theta_1=2\pi$, and generally will retain a double-humped appearance in a range of θ_x symmetric about $\theta_x=\pi$. Appendix A shows, moreover, that the double-humped condition occurs in regime

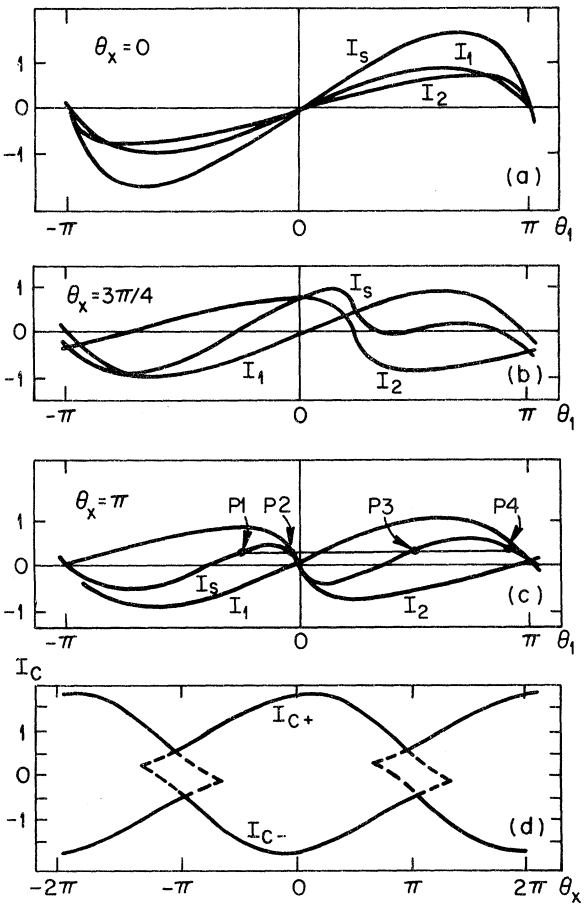

FIG. 5. (a) $I_1(\theta_1)$, $I_2(\theta_1+\theta_x)$, and $I_s(\theta_1, \theta_x)$ for $I_{c1}=1.0$, $I_{c2}=0.8$, $\alpha_1=0.4$, $\alpha_2=0.8$, and $\theta_x=0$. (b) Same except $\theta_x=\frac{3}{4}\pi$. (c) Same except $\theta_x=\pi$. The points P_1–P_4 are four points of $I_s(\theta_1, \pi)$ having the same value. (d) Solid lines—positive and negative critical currents. Dotted lines—positions of intermediate extrema of $I_s(\theta_1, \theta_x)$.

C as well.

If the function $I_s(\theta_1, \theta_x)$ does possess a double maximum and minimum then for some I_t there are four possible solutions to (11), e.g., the points P_1 to P_4 in Fig. 5(c), of which only the two corresponding to $dI_s(\theta_1, \theta_x)/d\theta_1 \geq 0$, e.g., P_1 and P_3, are stable solutions. (See Sec. III concerning the stability of these solutions and how transitions occur between them.) The critical current I_{c+} is again the maximum value of $I_s(\theta_1, \theta_x)$, corresponding to the higher of the two maxima. Now one can show (Appendix A) that if a double maxima occurs there is a θ_x, call it θ_x', at which the two maxima have equal heights. The rate of change of the heights with θ_x at $\theta_x = \theta_x'$, however, is different, so that for $\theta_x \lessapprox \theta_x'$, I_c will correspond to the maximum at smaller θ_1, and $dI_c/d\theta_x$ will have some value $(dI_c/d\theta_x)_<$, while for $\theta_x \gtrapprox \theta_x'$, I_c will switch to the maximum at larger θ_1 and will have a different slope $(dI_c/d\theta_x)_> \neq (dI_c/d\theta_x)_<$. The appearance of $I_s(\theta_1, \theta_x)$ in these two cases corresponds to Figs. 5(b) and 5(c). As a result the $I_c(\theta_x)$ has a break in slope at $\theta_x = \theta_x'$, or, if $(dI_c/d\theta_x)_<$ and $(dI_c/d\theta_x)_>$ have opposite signs, then $I_c(\theta_x)$ will have a cusplike minimum as in our example, Fig. 5(d), solid lines. Immediately on either side of the cusp or break in slope at $I_t = I_c$ the values of $I_1(\theta_1)$ and $I_2(\theta_2)$ are quite different. There is no formula, to our knowledge, for determining the position and depth of cusplike minima, but if there is only a break in slope the minimum is still at $I_c = I_{c1} - I_{c2}$ and $\theta_x = \pi - (\alpha_2 + \alpha_1)$ as in the first example.

Consider how the $I_c(\theta_x)$ changes as one passes continuously from regime A to regimes C and B. In Fig. 6, we show $I_c(\theta_x)$ for a case in which $I_{c2}/I_{c1} = 0.2$ and $\alpha = 0.5$, 0.7, 0.8, 0.9, passing from regime A to C and then B. In A it turns out that the point of maximum curvature or $d^2I_c/d\theta_x^2$ occurs on the steeply sloped portion just above the minimum of I_c. This maximum value of $d^2I_c/d\theta_x^2$ increases with increasing α until it becomes infinite at the boundary of the regimes A and C. The break in slope develops in $I_c(\theta_x)$ at this point. For an interval of larger α this break in slope remains above the minimum, so that one can still determine I_{c2} and α_2 from the position of the minimum. This condition persists throughout regime C and slightly into B. As one reaches the region bounded by the light line marked S-C in Fig. 3, however, the break in slope moves down, obscuring the rounded minimum and becoming itself the cusplike minimum. Note that even here one can still resolve the point of maximum descending slope of $I_c(\theta_x)$, corresponding to $I_2 = 0$ and having the value $I_{c2}/(1 + \alpha_2)$.

Returning to Fig. 5(d), the solid lines show $I_{c+}(\theta_x)$ and $I_{c-}(\theta_x)$, these corresponding, respectively, to the highest maximum and lowest minimum of

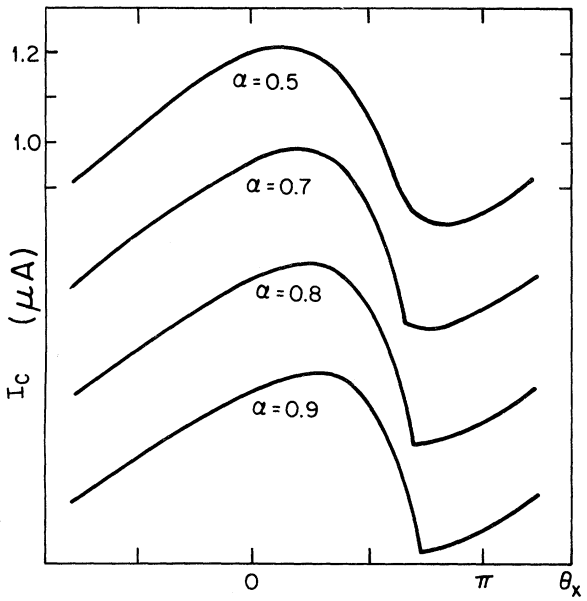

FIG. 6. $I_c(\theta_x)$ for the case $I_{c1} = 1.0$, $I_{c2} = 0.2$, $\alpha_1 = 0$, and $\alpha_2 = 0.5$, 0.7, 0.8, and 0.9. The latter three cases are offset vertically.

$I_s(\theta_1, \theta_x)$. We also show by dotted lines the continuations of the intersecting segments of the I_c which are the positions of the intermediate maxima and minima. These merge and vanish as $I_s(\theta_1, \theta_x)$ changes from double humped to single humped at some θ_x. Note here the characteristic asymmetry of the $I_c(\theta_x)$. Note also in this figure what happens when one begins with a situation in which $I_s(\theta_1, \theta_x)$ is double humped and then follows the positions of the two maxima through a cycle of θ_x. One sees the left-hand maximum at smaller θ_1 disappear while the right-hand maximum moves over to take its place with a third new maximum appearing and moving into the right-hand position. Thus the double maxima are in a sense the same maximum observed at two different states, corresponding to an increase in θ_x of 2π.

Third example. This case, shown in Fig. 7, involves still larger values of α_1 and α_2, $\alpha_1 = 16$, $\alpha_2 = 2$, $I_{c1} = 1.0$, and $I_{c2} = 0.6$ so that $I_{c2}/I_{c1} = 0.6$ and $\alpha = 11.6$. Consequently the $I_1(\theta_1)$ and $I_2(\theta_2)$ shown in Figs. 7(a) and 7(b) are reentrant and multivalued. We shall see in Sec. III that the reentrant portions of the $I(\theta)$ are dynamically unstable and a static state always corresponds to the nonreentrant portion of the $I(\theta)$ curves. Consequently we delete these reentrant portions in the remainder of Fig. 7.

In forming the sum $I_s(\theta_1, \theta_x)$ for the graphical solution of (11) for multivalued $I(\theta)$ the procedure is to add to each branch of one function all overlapping branches of the other. In Fig. 7, in which the various branches of the $I(\theta)$ are in a sense

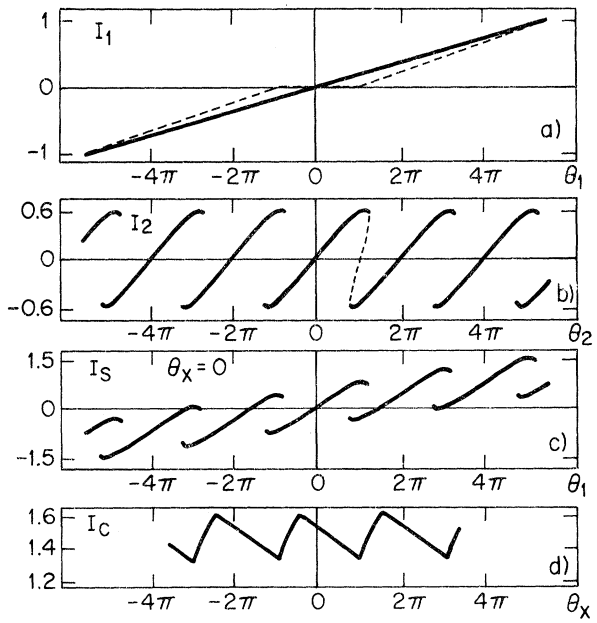

FIG. 7. (a) $I_1(\theta_1)$ for $I_{c1}=1.0$ and $\alpha_1=16$. Dotted lines show the reentrant portions of $I_1(\theta_1)$. (b) $I_2(\theta_2)$ for $I_{c2}=0.6$ and $\alpha_2=2$. Dotted line shows one reentrant portion of $I_2(\theta_2)$. (c) $I_s(\theta_1, \theta_x)$ for $\theta_x=0$. (d) $I_c(\theta_x)$.

portions of the same continuous branch separated by $\Delta\theta=2\pi$, it is equivalent and convenient to plot a single branch of $I_1(\theta_1)$ in an extended range of $\theta_1>2\pi$ and to add to it each of the branches of I_2 where they overlap. This is done in Fig. 7(c) for $\theta_x=0$. Here again the multiple maxima correspond in a sense to a single maximum observed at succesive values of θ_x separated by 2π.

The largest maximum of $I_s(\theta_1, \theta_x)$ is I_{c+} and a plot of $I_{c+}(\theta_x)$ is shown in Fig. 7(d). It resembles the $I_{c+}(\theta_x)$ of Fig. 5 in the asymmetry and cusplike minima. Here, however, less indication of the sinusoidal curvature remains than in Fig. 5. In the limit of very large α_1 and α_2 I_{c+} has a nearly saw-tooth shape, with slopes $dI_{c+}/d\theta_x \approx I_{c2}/\alpha_2=\Phi_0/2\pi L_2$ and $dI_{c+}/d\theta_x \approx -I_{c1}/\alpha_1=-\Phi_0/2\pi L_1$ on the ascending and descending portions of the curve, respectively, leading to variations in I_c of Φ_0/L to lowest order. In this regime when $I_t \ll I_c$ the values of $\phi_2-\phi_1$ are rather close to a multiple of 2π for the states in which $|I_2| \ll I_{c2}$ and $|I_1| \ll I_{c1}$. In this case the flux $\Phi=\Phi_s+\Phi_x$ occurs in near multiples of Φ_0, i.e., is nearly quantized. If either I_1 and I_2 approaches its critical value, however, the approximate flux quantization no longer holds.

B. Mechanical Analog of Double Junction

For many Josephson problems there are mechanical systems, often involving the simple pendulum, whose equations of motion have the same form. For the double junction such an analog is the double pendulum sketched in Fig. 8(a). The two pendulums 1 and 2 whose angular positions are β_1 and β_2, measured from vertically downward, are capable of exerting gravitational torques $M_1 \sin\beta_1$ and $M_2 \sin\beta_2$, where $M_2 \leq M_1$. They are connnected by a torsion bar of stiffness K with a built-in angular displacement of β_x, that is, in the absence of gravity or externally applied torque the torsion bar is unstressed and the pendulums would have an angular separation of $\beta_2-\beta_1=\beta_x$. There is an external torque τ_x applied at a point Q on the torsion bar at a distance X_1 from pendulum 1 and X_2 from pendulum 2. The sign conventions are shown in Fig. 8(a). Both the statics and the dynamics of this device have implications for the double junction. We consider in this section only the statics, discussing the dynamics in Sec. III. In the static case the external and gravitational torques are in balance, leading to

$$\tau_x = M_1 \sin\beta_1 + M_2 \sin\beta_2 \ . \tag{12}$$

The torque-induced twist in the torsion bar between the point Q and pendulum 2 is $-(X_2 M_2/K)\sin\beta_2$, and that between pendulum 1 and point Q is $(X_1 M_1/K)\sin\beta_1$, the total torque-induced

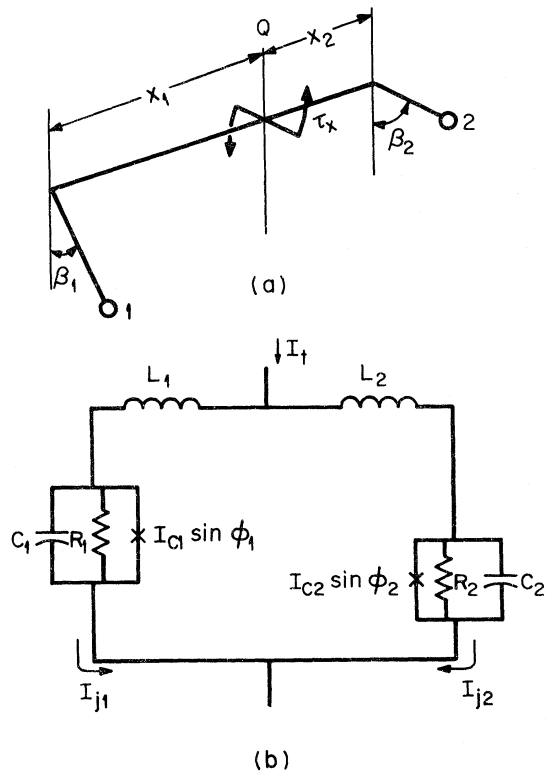

FIG. 8. (a) Double pendulum connected by torsion bar—mechanical analog of the double junction. (b) Equivalent circuit of the double junction in the dynamical case.

twist β_s being the sum of these. The actual displacement between β_2 and β_1 is the built-in displacement β_x plus β_s or

$$\beta_2 - \beta_1 = \beta_x + (X_1 M_1/K)\sin\beta_1 - (X_2 M_2/K)\sin\beta_2 \ . \tag{13}$$

Equations (12) and (13) are of the same form as (1) and (5) for sinusoidal $I(\phi)$ so the statics of the double pendulum and double junction are completely analogous. The quantities (ϕ_i, $\sin\phi_i$, I_{ci}, I_i, $2\pi L_i/\Phi_0$, $2\pi\Phi_x/\Phi_0$, $2\pi\Phi_s/\Phi_0$, I_t) in the double junction correspond, respectively, to the quantities (β_i, $\sin\beta_i$, M_i, $M_i\sin\beta_i$, X_i/K, β_x, β_s, τ_x) in the mechanical problem. Note that I_c corresponds to the maximum static torque that the pendulums can balance for a fixed value of β_x, a quantity we shall denote τ_c.

An analysis similar to that in Sec. IIA can also be used in the mechanical case. The analogous quantities to the $I(\theta)$ have a direct mechanical interpretation. Suppose $\tau_x = 0$ and $\beta_x = 0$ so that $\beta_1 = 0$. If the torsion bar at Q is rotated through an angle γ_1, pendulum 1 will rotate through a corresponding angle β_1 and develop a gravitational torque τ_1. The function relating τ_1 to γ_1 is the analogous quantity to $I_1(\theta_1)$, and a similar interpretation holds for $\tau_2(\gamma_2)$. For example, for a rigid torsion bar $\tau_1(\gamma_1)$ is a sinusoid whereas for a less stiff bar the pendulum can sag, requiring an extra rotation of the torsion bar beyond $\frac{1}{2}\pi$ to bring it into the horizontal position. This leads to a skewed sinusoidal torque-angle relation $\tau_1(\gamma_1)$, in analogy to the skewness of $I_1(\theta_1)$ when $L_1 \neq 0$. If the torsion bar is sufficiently nonrigid the pendulum cannot be made to stand vertically upright while remaining stable, a situation corresponding to a reentrant $I_1(\theta_1)$. Nonetheless, the same interpretation holds with the reentrant position corresponding to the position of unstable mechanical equilibrium.

Let us consider briefly the previous examples as they appear in this analog. The case of Fig. 4 corresponds to a situation in which M_1X_1/K and M_2X_2/K are small; i.e., the torsion bar is stiff enough that the two pendulums are almost rigidly attached with only a slight sag occurring, the sag clearly being more pronounced when either pendulum is nearly horizontal. Indeed the torsion bar is stiff enough that when $\beta_x = \pi$ and $\tau_x = 0$ the lighter pendulum will stand vertically upright at $\beta_2 = \pi$ and the torsion bar will remain untwisted. As, say, K is decreased or M_2 is increased a point will be reached, for $\beta_x = \pi$ and $\tau_x = 0$, at which for small changes in β_2 the energy gained from gravity and the energy required to twist the bar will just balance. The upright position of the lighter pendulum thus becomes unstable, and the pendulum will flop over to one side or the other. This situation corresponds to $I_{c2}/I_{c1} + \alpha = 1$, the boundary between regimes C and B in Fig. 3. (Actually for $\tau_x \neq 0$ double-valued behavior sets in somewhat sooner, at the boundary between C and A.) The two stable positions for the pendulum at $\beta_x = \pi$, $\tau_x = 0$ correspond in the double junction to the fact that there are two stable conditions for $I_t = 0$, $\theta_x = \pi$ if $\alpha + I_{c2}/I_{c1} \geq 1$, i.e., a type-$B$ case as in Fig. 5. For still larger M_1X_1/K and M_2X_2/K the pendulums are sufficiently heavy and the torsion bar sufficiently weak that for small values of τ_x there are several static states. These are set up by holding one pendulum fixed and giving the other some integral number of 2π rotations, and then allowing both pendulums to find their equilibrium position. If the pendulums are heavy enough these twisted positions will be stable. This corresponds to the regime of Fig. 7, and the various branches of the $I_s(\theta_1, \theta_x)$ correspond to the branches of the $\tau_s(\gamma_1, \beta_x) = \tau_1(\gamma_1) + \tau_2(\gamma_1 + \beta_x)$ with each branch representing a different "trapped-twist" situation. As M_1X_1/K and M_2X_2/K become very large the trapped twists occur in near multiples of 2π, corresponding to the regime of nearly complete fluxoid quantization in in the double junction.

III. DYNAMICS OF DOUBLE JUNCTION

A model circuit for a single small Josephson junction has been discussed by Stewart[16] and by McCumber.[17] Their model, appropriate for small junctions and low voltages, comprises a parallel circuit of the junction capacitance C, a resistance R simulating the dissipative mechanism, and an element supporting a supercurrent $I_c\sin\phi$. The current continuity equation combined with Josephson's relation $V = \Phi_0(d\phi/dt)/2\pi$ leads to an equation describing the dynamics which has the form of Newton's law for a driven damped single pendulum. For the double junction a similar model circuit is shown in Fig. 8(b). It consists of two Stewart-McCumber circuits connected in parallel through inductances L_1 and L_2, with current I_t fed between the two inductances. The assumption here is that the capacitance between the two bulk superconductors can be localized in the region of the junction, a good approximation for tunnel junctions, and that the dissipative currents flow only through the two junctions and can be adequately simulated as Ohmic, although for tunnel junctions this is a crude approximation. The current continuity equation for this system is

$$I_t = I_{j1} + I_{j2} \ , \tag{14}$$

where I_{j1}, the current in L_1, includes contributions from the displacement current and dissipative current as well as the supercurrent, with a similar interpretation of I_{j2}. Specifically, we have

$$I_{j1} = I_{c1}\sin\phi_1 + \frac{\Phi_0}{2\pi R_1}\frac{d\phi_1}{dt} + \frac{\Phi_0 C_1}{2\pi}\frac{d^2\phi_1}{dt^2} \ , \tag{15}$$

$$I_{j2} = I_{c2}\sin\phi_2 + \frac{\Phi_0}{2\pi R_2}\frac{d\phi_2}{dt} + \frac{\Phi_0 C_2}{2\pi}\frac{d^2\phi_2}{dt^2}\ , \qquad (16)$$

where we have used $d\phi_1/dt = 2\pi V_1/\Phi_0$ and $d\phi_2/dt = 2\pi V_2/\Phi_0$, V_1 and V_2 being the respective voltages across the two junctions. Equating the voltage drop around the circuit to $d\Phi_x/dt$ and integrating with respect to time, we obtain

$$\phi_2 - \phi_1 = 2\pi\Phi_x/\Phi_0 + L_1 I_{j1} - L_2 I_{j2}\ , \qquad (17)$$

where Φ_x is the external magnetic flux and, we reemphasize, I_{j1} and I_{j2} contain contributions not only from the supercurrents but also from the displacement and dissipative currents.

There is a direct analogy between (14)–(17) and the equations which define the motion with time of the double pendulum. For the latter, in addition to the quantities defined in Sec. IIB, we have the moments of inertia A_1 and A_2 of each pendulum and we assume that each pendulum is subject to a drag torque proportional to the angular velocity given by $-B_1 d\beta_1/dt$ and $-B_2 d\beta_2/dt$. We neglect any inertial properties or drag related to the torsion bar (but it is worth noting that inclusion of these would be analogous to including electromagnetic resonances between the two bulk superconductors). The pendulums are subject to respective torques τ_1 and τ_2 transmitted to them by the torsion bar. Newton's law for the two takes the forms

$$\tau_1 = M_1\sin\beta_1 + B_1\frac{d\beta_1}{dt} + A_1\frac{d^2\beta_1}{dt^2}\ , \qquad (18)$$

$$\tau_2 = M_2\sin\beta_2 + B_2\frac{d\beta_2}{dt} + A_2\frac{d^2\beta_2}{dt^2}\ . \qquad (19)$$

The external torque balances τ_1 and τ_2, so that we have

$$\tau_x = \tau_1 + \tau_2\ . \qquad (20)$$

The instantaneous angular displacement $\beta_2 - \beta_1$ is given by the built-in displacement β_x plus any torque-induced twist in the torsion bar due to τ_1 and τ_2. This leads to the constraint

$$\beta_2 - \beta_1 = \beta_x + X_1\tau_1/K - X_2\tau_2/K. \qquad (21)$$

We emphasize that τ_1 and τ_2 are not solely gravitational but contain inertial and damping forces as well.

Equations (18)–(21) fully determine the motion of the double pendulum and have the same form as (14)–(17) for the double junction. The two systems are then complete analogs. To complete our previous list of corresponding quantities we add $[\Phi_0 C_i/2\pi,\ \Phi_0/2\pi R_i,\ I_{ji},\ I_s(\theta_1,\theta_x),\ I_c(\theta_x)]$ for the junction corresponding to $[A_i,\ B_i,\ \tau_i,\ \tau_s(\gamma_1,\beta_x),\ \tau_c(\beta_x)]$ for the pendulum. We may point out that situations in which the pendulums are (i) static, (ii) oscillating about some average positions with a time average of $d\beta_1/dt$ and $d\beta_2/dt$ of zero, or (iii) rotating repeatedly through complete cycles with a nonzero time average of $d\beta_1/dt$ and $d\beta_2/dt$ correspond, respectively, in the double junction to situations of (i) zero voltage, (ii) voltage oscillations with zero time average voltage, and (iii) nonzero dc voltage situations.

It would require too much space to attempt to discuss all the various time-dependent phenomena which occur in double junctions, even for this simplified model, although several novel effects occur which we hope to describe elsewhere. We consider here only features relevant to the quasistatic properties, particularly I_c. The effect of the dynamics can be illustrated by using the examples of Figs. 4, 5, and 7. We phrase the discussion in terms of measuring τ_c in the pendulum analog. We assume that τ_c is determined by beginning at $\tau_x = 0$ and slowly increasing τ_x until the pendulum is finally set into steady-state rotation at $\tau_x = \tau_c$. This corresponds to the manner of measuring I_c in our experiments.

We begin with a type-A case, i.e., $M_1X_1/K \ll 1$ and $M_2X_2/K \ll 1$. For $\tau_x = 0$, the pendulums are at rest at angles dictated by β_x. As τ_x is increased slowly the pendulums adjust their angle adiabatically until they reach the maximum gravitational torque they can provide for the particular β_x. A further increase in τ_x causes them to "overbalance" and sets them into a steady state of rotation. For τ_x applied sufficiently slowly the gravitational torque is always in balance with τ_x and (12) and (13) are obeyed. Similarly, in measuring I_c the double junction follows $I_s(\theta_1, \theta_x)$ if I_t is changed slowly with respect to the small oscillation period.

Note that an applied torque could in principle hold the pendulum at the positions of unstable equilibrium, with the pendulums above the horizontal, as well as at the stable position. These unstable equilibria are just the positions which correspond to the solutions of $I_t = I_s(\theta_1, \theta_x)$ which lie on the portions of $I_s(\theta_1, \theta_x)$ having negative slope, e.g., P_2 in Fig. 4(a), which justifies our previous remark that such positions are not stable solutions. Similarly, the instability of the solutions which correspond to reentrant portions of the $I(\theta)$ corresponds to the fact that a pendulum whose $\tau(\gamma)$ is reentrant cannot be put into a stable vertically upright position by torque applied at Q.

Consider next the case in which M_1X_1/K and M_2X_2/K are increased and β_x is adjusted so that $\tau_s(\gamma_1, \beta_x)$ has a double maximum and minimum, as in Fig. 9(a). The dynamics of this case have two different regimes which we discuss in turn.

In the first regime $\tau_s(\gamma_1, \beta_x)$ has a double maximum but the secondary mininum lies at $\tau_s(\gamma_1, \beta_x) > 0$, so that as in Fig. 9(a) there is only one stable state at $\tau_x = 0$, γ_{1A} in Fig. 9(a). This is always the

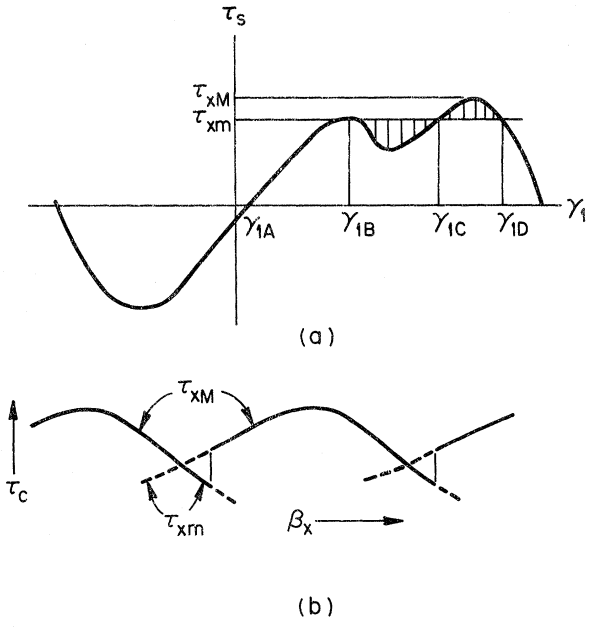

FIG. 9. (a) $\tau_s(\gamma_1, \beta_x)$ for a double pendulum of case B or C with one stable state at $\tau_x = 0$. For zero damping the jump at τ_{xm} is unstable and $\tau_c = \tau_{xm}$. (b) Solid lines—$\tau_c(\beta_x)$ for small damping. Dotted lines—position of the other maxima of $\tau_s(\gamma_1, \beta_x)$.

case for all β_x in a type-C regime (see Appendix A), and is the case for some but not all of the range of β_x in a type-B regime. As τ_x is slowly increased γ_1 increases from γ_{1A}, following the curve $\tau_s(\gamma_1, \beta_x)$. When τ_x reaches τ_{xm} corresponding to the first maximum at $\gamma_1 = \gamma_{1B}$ in Fig. 9(a), however, the system can follow the curve no farther. At this point one pendulum, say the first, has been tilted to $\beta_1 = \frac{1}{2}\pi$ or slightly farther. A further increase in τ_x will cause that pendulum to overbalance and begin to rotate. Once this occurs there are several possibilities. If viscous damping is large the inertial effects are not important and, once overbalanced, the first pendulum and the second will slowly relax to new equilibrium positions corresponding to $\gamma_1 = \gamma_{1C}$ in Fig. 9(a), in which τ_2 is increased and τ_1 is decreased. From this point a further adiabatic increase in τ_x will cause the system to follow the curve to the largest value τ_{xM} beyond which the pendulums are set into rotation, so that $\tau_c = \tau_{xM}$. If damping is small and inertial effects are important there are two possibilities. Once pendulum 1 begins to rotate under the constant applied torque τ_{xm} it acquires kinetic energy and in consequence it overshoots the static position $\gamma_1 = \gamma_{1C}$. In effect the nonadiabatic change in position of the pendulum excites the oscillations of the system. It is apparent that if this kinetic energy is too small it cannot overcome the energy barrier which must be surmounted in order for the pendulums to be set into rotation. (The magnitude of the energy barrier is derived in Appendix B.) Instead the pendulums undergo coupled oscillations which ultimately are damped out, the system coming to rest at $\gamma_1 = \gamma_{1C}$. We call this process, in which the system shifts in this fashion from one γ_1 to another without causing rotation to begin, a stable jump. Following a stable jump the double pendulum follows $\tau_x = \tau_s(\gamma_1, \beta_x)$ to $\tau_x = \tau_{xM}$ beyond which it begins to rotate. On the other hand, if the kinetic energy acquired in the flipping of pendulum 1 is sufficient to overcome the energy barrier and the damping losses, a situation we call an unstable jump, pendulums will begin to rotate at $\tau_x = \tau_{xm}$. Obviously the smaller τ_{xm} is compared to τ_{xM} and the higher the damping the more likely the jump is to be stable. It turns out in fact (Appendix B) that in the zero-damping limit the area under $\tau_s(\gamma_1, \beta_x)$ and $I_s(\theta_1, \theta_x)$ determines the stability of the jump. In Fig. 9(a), the energy "saddle point" for $\tau_x = \tau_{xM}$ corresponds to the unstable point $\gamma_1 = \gamma_D$. Considering the two cross-hatched areas in Fig. 9(a), if the area below the line $\tau_x = \tau_{xm}$ is larger than that above the line the jump is unstable and vice versa. In Fig. 9(a), the jump is clearly unstable in the absence of damping. In the double junction an analogous situation occurs. The absence of damping in a junction is related to hysteresis of its I-V curve.[16,17] For highly damped junctions (these with nonhysteretic I-V curves, e.g., superconductor–normal-metal–superconductor sandwiches[18] or, in our experience, point contacts) the measured I_c always occurs at the largest value of $I_s(\theta_1, \theta_x)$, I_{cM} (corresponding to τ_{xM}). In underdamped junctions (e.g., tunnel junctions[16,17]), however, the measured I_c might or might not occur at a secondary maximum I_{cm} (corresponding to τ_{xm}) depending on whether the jump involved is stable or not. Figure 9(b) shows schematically the $I_c(B)$ curves in the undamped cases, the solid lines showing the observed I_c and the dotted lines the positions of the other maxima.

In the second double-maximum case $\tau_s(\gamma_1, \beta_x)$ appears as in Fig. 10(a), with maxima at τ_{xm} and τ_{xM} as before, but where now the secondary minimum is negative, providing the new element of two possible stable states at $\tau_x = 0$. Once again to measure τ_c we start at $\tau_x = 0$ and increase τ_x until rotation sets in. In this process the system could initially be either at γ_{1A} or γ_{1B}, in Fig. 10(a), depending upon previous history. For heavy damping the observed τ_c will be τ_{xM} as before, irrespective of the initial state. For light damping if $\gamma_1 = \gamma_{1A}$ initially, the system will follow $\tau_s(\gamma_1, \beta_x)$ to τ_{xm} and the jump takes place as before, the choice between τ_{xm} and τ_{xM} as τ_c depending on whether the jump is stable or unstable. If, however, $\gamma_1 = \gamma_{1B}$

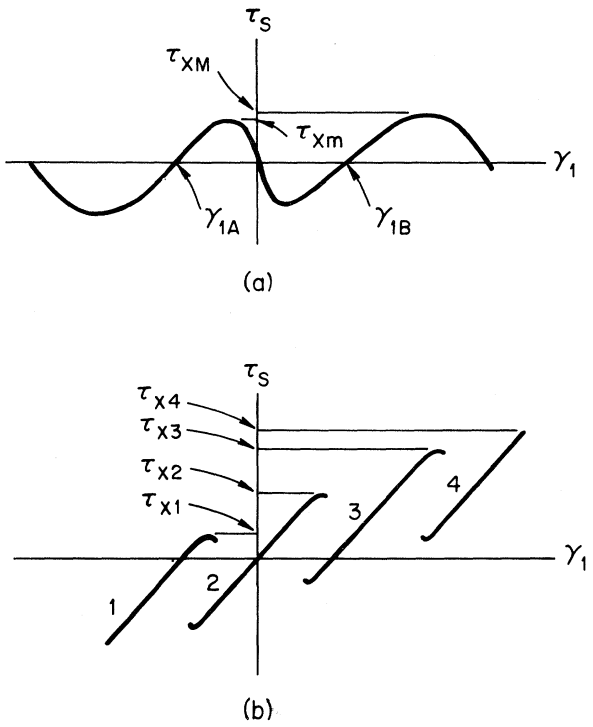

FIG. 10. (a) $\tau_s(\gamma_1, \beta_x)$ for a double pendulum of case B or C with two stable states at $\tau_x = 0$. (b) $\tau_s(\gamma_1, \beta_x)$ for a double pendulum having three possible states at $\tau_x = 0$ and three jump possibilities.

initially then no jump is involved and the observed τ_c is τ_{xM}. Similarly for the heavily damped double junction I_{cM} is always the observed critical current but for lightly damped junctions either I_{cm} or I_{cM} may be observed in cases where the jump is unstable, depending upon which initial configuration is selected by the junction. In this case one can experimentally follow the position of a maximum of $I_s(\theta_1, \theta_x)$ even if it is not the highest.

In the final example consider an extension of this situation corresponding to the $\tau_s(\gamma_1, \beta_x)$ shown in Fig. 10(b), which is similar to the $I_s(\theta_1, \theta_x)$ shown in Fig. 7. Here there are four relative maxima, τ_{x1}–τ_{x4} being, respectively, the highest points on branches 1–4, and there are three stable states at $\tau_x = 0$, on branches 1–3. Following the previous arguments any of the τ_{x1}–τ_{x4} might be the observed τ_c depending on circumstances. In heavily damped cases $\tau_c = \tau_{x4}$ is always observed as all jumps are stable. As an example of a lightly damped case, suppose the jump at τ_{x1} is stable but those at τ_{x2} and τ_{x3} are not. Then one might expect only to observe τ_{x2} or τ_{x3} as τ_c, since there is no stable state on branch 4 at $\tau_x = 0$. The stable jump at τ_{x1} need not necessarily end up on branch 2, however, but might well be energetically able to reach branches 3 or 4. If so, which branch is the ultimate steady state reached by the jump at τ_{x1} depends in a complex way on the interplay of the damping and the internal oscillations of the pendulum, and the result can probably be regarded as random, with differing probabilities for each branch. If branch 4 can be reached by a stable jump, then $\tau_c = \tau_{x4}$ would also be observed in some cases in which the initial state was on branch 1.

In this example the various maxima of $\tau_s(\gamma_1, \beta_x)$ are, as previously discussed, in essence the same maximum observed at intervals of β_x separated by 2π. For $\tau_c(\beta_x)$, then, the dependences of τ_{x1}, τ_{x2}, τ_{x3}, and τ_{x4} on β_x are identical, but offset by $\Delta\beta_x = 2\pi$.

In the double junction, the measurement of I_c generally involves switching from $V = 0$ to $V \neq 0$ and back by repeatedly sweeping the current bias symmetrically on either side of $I_t = 0$, the junction returning to $V = 0$ at some current (which for tunnel junctions is $I_t \approx 0$). If at this current bias there are several stable states the junction may end up in any of them at random, although with unequal probabilities, as the choice depends in a complex and uncontrollable way on the details of the current sweep. Thus in a lightly damped junction one will observe multiple critical currents with identical dependences on B but displaced by one period each. In this example these would correspond to τ_{x2} and τ_{x3}, and perhaps τ_{x4}. For large α_1 these would be spaced by approximately Φ_0/L_1.

To summarize the implication of the dynamics: (i) For heavily damped junctions (such as *SNS* or probably point contacts) the $I_c(B)$ will be as described in Sec. II. (ii) For lightly damped junctions (such as the tunnel junctions of Sec. IV) the $I_c(B)$ for type A are as described in Sec. II. If α and I_{c2}/I_{c1} are large enough, however, that cusp-like features would occur in damped junctions, then either $I_c(B)$ will show a discontinuous jump at these points rather than a cusp, or multiple I_c will be observed each having an identical dependence on B except for a fixed displacement in B corresponding to $\theta_x = 2\pi$. Each of the multiple I_c can be observed so long as it corresponds to an unstable jump and disappears for values of B at which it is sufficiently reduced to correspond to a stable jump.

IV. EXPERIMENT

In this section we describe the results of experiments conducted on double junctions of a thin-film sandwich construction. Typically these are made as follows: A long (~ 2 cm) strip of Sn of width l (~ 0.5 cm) and thickness t_1 is deposited by vacuum evaporation and a slightly narrower, equally long strip of Ge of thickness t_{Ge} is superimposed upon it, leaving both edges of the Sn strip uncovered, the widths of the uncovered portions being a

and b. The combination is oxidized in an oxygen plasma discharge and subsequently five long narrow Sn strips of width w and thickness t_2 oriented at right angles to the large strip are deposited, giving five double junction loops with the Ge forming the filler material of the loop. Typical dimensions are a, b, and $w \sim 0.2$ mm, $l \sim 0.5$ cm, and film thicknesses determined by optical interference of 1000–10 000 Å. The inset of Fig. 11 shows the configuration.

The junctions are wired for four-terminal I-V measurements using one end of the cross strip and the broad strip as current leads, and are either immersed directly in liquid He or are mounted on a variable temperature holder which makes use of exchange gas and a resistance heater to warm the sample above the bath temperature. The junctions are shielded from the earth's field by a μ-metal can whose stray internal fields are $\lesssim 10^{-2}$ G. The magnetic field B is provided by a solenoid and is applied to the sample in a direction perpendicular to the area of the double junction loops.

The I-V curves of the junctions studied were typical of Sn-Sn tunnel junctions, displaying at low temperatures only small amounts of excess currents and subharmonic structure. To ensure that the junctions had current-phase relations which were basically sinusoidal it was necessary to have individual critical currents which were small enough (of order 1 mA) that self-field effects within the junctions were negligible. In the junctions which we describe these conditions were satisfied. Under such conditions the magnitude of the Josephson current will be nearly equal to the current rise at $V = 2\Delta$ ($2\Delta = 1.21$ mV for Sn), provided that no magnetic flux is trapped within the Sn films. The spreading of any such flux (quantized in minimum units of Φ_0) in the plane of a single junction, of course, substantially reduces the critical current. If such flux is trapped it is generally possible to purge it and restore the Josephson currents by warming the sample above the critical temperature briefly and allowing the sample to cool again in zero applied field with no applied current.

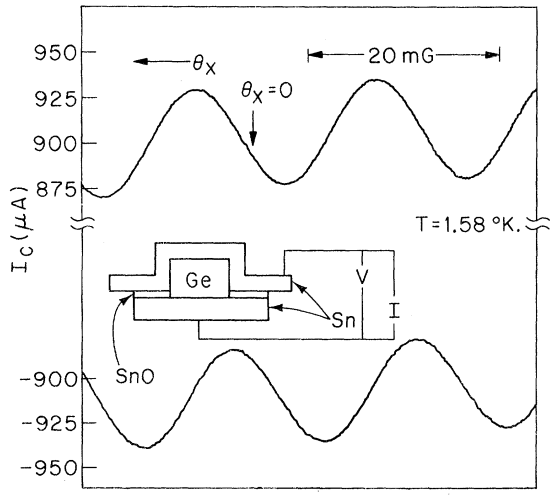

FIG. 11. Positive and negative $I_c(B)$ for a Sn-Sn double tunnel junction (inset). The position of $\theta_x = 0$ is deduced from the arguments of the text. In this figure and in Figs. 12–16 the values of I_c at the extrema of the fringes vary from one to the next as a result of the diffraction background. The values used in the analysis of the text are taken at corresponding extrema of I_{c+} and I_{c-} nearly at the diffraction peak.

The critical current I_c was measured as a function of B by displaying the I-V characteristic on a Tektronix 561 oscilloscope at a repetition rate of a few hundred Hz and utilizing a Pacific Electric Measurements CRT converter which in each sweep samples the applied current at the first onset of voltage and plots this value directly on one axis of an x-y recorder, with the current applied to the solenoid being plotted on the other axis.

The oscillatory $I_c(B)$ patterns measured in this fashion are a combined diffraction-interference pattern since the junctions are not actually of negligible size compared to the loop dimensions. The period of the oscillations ΔB measured at small B at the peak of the diffraction envelope may be characterized by a magnetic area $\bar{A}$, defined by $\bar{A} = \Phi_0/\Delta B$. In the absence of demagnetizing effects such as sample misalignment $\bar{A}$ should be given by[14]

$$\bar{A} = [d + \lambda_1 \tanh(t_1/2\lambda_1) + \lambda_2 \tanh(t_2/2\lambda_2)] \times (l + \tfrac{1}{2}a + \tfrac{1}{2}b) + t_{Ge} l \,, \quad (22)$$

which for $t_1 \gg \lambda_1$ and $t_2 \gg \lambda_2$ reduces to

$$\bar{A} = (d + \lambda_1 + \lambda_2)(l + \tfrac{1}{2}a + \tfrac{1}{2}b) + t_{Ge} l \,. \quad (23)$$

We have included here the possibility that $\lambda_1 \neq \lambda_2$ even though both films are of Sn. This situation is particularly likely to occur near the critical temperature, which varies from film to film in our samples from ~3.7 to ~3.8 °K. At low temperature we would expect that $\lambda \sim 500$ Å as others have observed for Sn films, and we use the usual approxproximate formula $\lambda(T) = \lambda(T=0)[1-(T/T_c)^4]^{-1/2}$ to estimate λ at higher temperatures.

As a first example we show in Fig. 11 the $I_c(B)$ interference pattern obtained for one such junction whose dimensions were $a = 0.11 \pm 0.01$ mm, $b = 0.39 \pm 0.02$ mm, $l = 4.19 \pm 0.03$ mm, $w = 0.37 \pm 0.01$ mm, $t_1 = 2400 \pm 200$ Å, $t_2 = 3700 \pm 100$ Å, and $t_{Ge} = 1000 \pm 200$ Å. The curves, taken at $T = 1.58$ °K, are shown for a ~50-mG range about $B = 0$ and possess a smooth continuous near-sinusoidal appearance, indicating that this is a type-A case

corresponding to Fig. 4. Over a larger field, $\sim\frac{1}{2}$ G, a diffraction background characteristic of the individual magnetic field dependence of I_{c1} and I_{c2} modulates the interference pattern, but in Fig. 11 this provides only a slight curvature of the pattern. Both $I_{c+}(B)$ and $I_{c-}(B)$ are shown, the current scale being broken in order to do so. Note that the two have the same shape with only a phase shift between them, thus satisfying the previously mentioned time-reversal requirement.

The parameters I_{c1}, I_{c2}, α_1, and α_2 can be extracted from the curves as follows. The maximum I_c, I_{cM} (ignoring the background curvature) is $I_{cM} = 934 \pm 1$ μA and the modulation depth ΔI is 55.7 ± 1 μA. For this type-A case we have $I_{c2} = \Delta I/2 = 27.8 \pm 0.5$ μA and $I_{c1} = I_{cM} - I_{c2} = 906.3 \pm 1.3$ μA. The angular separation $\Delta\theta_x$ between the maximum and minimum of, say, I_{c+} expressed as a fraction of one period (2π) is $\Delta\theta_x/2\pi = 0.500 \pm 0.013$, i.e., $I_c(B)$ is essentially symmetric. Hence $\alpha_2 = (\Delta\theta_x/2\pi - \frac{1}{2})\pi = (0 \pm 0.013)\pi = 0 \pm 0.05$ and consequently $L_2 = \alpha_2\Phi_0/2\pi I_{c2} = 0 \pm 0.6 \times 10^{-12}$ H. The measured maximum and minimum slopes are 27.6 ± 1 μA/rad in agreement with $\pm I_{c2}/(1 \pm \alpha_2) = 27.8 \pm 0.5$ μA/rad.

The determination of α_1 is somewhat more indirect. The phase displacement $\delta\theta_x$ between the maxima of I_{c+} and I_{c-}, expressed as a fraction of a period (2π), is $\delta\theta_x/2\pi = \pm(0.29 \pm 0.02)$. Here the initial $\pm$ indicates that the sense of increasing θ_x is not known. Ordinarily this sense is obvious for a type-A interference pattern from the asymmetry of the slopes of I_c, namely, θ_x increases in that direction for which I_{c+} increases gently and decreases steeply. This sign convention can be traced back to the original assumptions that $I_{c2} \leqq I_{c1}$ and $\phi_2 - \phi_1 = 2\pi\Phi/\Phi_0$. In this case, however, there is no noticeable asymmetry in the slopes. There is a further uncertainty of $2n\pi$ ($n = 0, \pm 1, \pm 2$, etc.) because an increase in α_1 by 2π would produce the same apparent phase shift $\delta\theta_x$ between I_{c+} and I_{c-}. From the $I_c(B)$ alone without further information one can only conclude that $\delta\theta_x/2\pi$ is one of the set of numbers $(\pm n \pm 0.29)\pi$.

Now because we found that $\alpha_2 \approx 0$ and $L_2 \approx 0$, one must have $L_1 > 0$ and $\alpha_1 > 0$ because $L_1 + L_2 = L > 0$. We can therefore rule out the positive values of $\delta\theta_x = 2\alpha_2 - 2\alpha_1$. Another sometimes helpful condition on α_1 is the inequality $I_{c2}/(1 - \alpha_2) < I_{c1}/(1 + \alpha_1)$ which holds for type-A patterns. This is most useful, however, if $I_{c2}/I_{c1} \gtrsim 0.1$ and for this case it gives only the weak constraint $\alpha_1 < 30$ or $\delta\theta_x/2\pi < 10$. To finally pin down α_1 we calculate the inductance L. In this thin-film configuration we can compute L if we assume that the broad lower strip acts as a ground plane, concentrating the current flow in the narrow upper strip on the under surface, between the two Sn strips. A general formula for L in this case,[19] assuming a and b are small compared to l, is

$$L = (\mu_0/W)\{(l + \tfrac{1}{2}a + \tfrac{1}{2}b) \times [\lambda_1 \coth(\lambda_1/t_1) + \lambda_2 \coth(\lambda_2/t_2) + d] + lt_{Ge}\}, \quad (24)$$

which, for the limit $t_1 \gg \lambda_1$ and $t_2 \gg \lambda_2$, appropriate in this case, becomes $L = \mu_0\bar{A}/W$. Using the observed $\Delta B = 20.1 \pm 0.1$ mG we obtain $\bar{A} = 1.03 \pm 0.005 \times 10^{-5}$ cm^{-2}. [We note that $\lambda_1 + \lambda_2 + d$ can be calculated from $\bar{A}$ and the dimensions a, b, l, and t_{Ge} from (23), giving in this case $\lambda = 700 \pm 200$ Å. The usually quoted value for Sn at $T = 0$ is 510 Å for pure Sn, with increasing values for samples of shorter mean free path.] From $\bar{A}$ we obtain $L = 3.5 \pm 0.1 \times 10^{-12}$ H. Taking $L_2 = 0$, $L_1 = L$ we obtain $\alpha_1 = 2\pi L_1 I_{c1}/\Phi_0 = (3.06 \pm 0.08)\pi$, in rough agreement with one of the possible values of $\delta\theta_x/2\pi = \alpha_2 - \alpha_1 = (\pm n \pm 0.29)\pi$. Taking $n = 3$, then, the measured $\alpha_1 = (3.29 \pm 0.01)\pi$ implies the value $L_1 = 3.75 \pm 0.1 \times 10^{-12}$ H, which together with $L_2 = 0.0 \pm 0.5 \times 10^{-12}$ H is in fair accord with the computed L. This choice incidentally determines the direction of increasing θ_x in Fig. 11 as being to the left.

Calculation of the relative values of L_1 and L_2 depends upon the precise form of the current flow patterns in the superconducting films. Since the current is fed to one end of the broad strip and is removed from one side of the narrow strip, however, one or the other of L_1 and L_2 should be much larger than the other. In this case $L_1 \gg L_2$ which indicates that the junction having the smaller critical current is on that side of the interferometer from which the current is removed from the cross strip.

It is noteworthy that for these values, $I_{c2}/I_{c1} = 0.03$ and $I_{c1}/(1 + \alpha_1) = 2.9[I_{c2}/(1 - \alpha_2)]$, the plot of $I_c(\theta_x)$ should be an accurate representation of $I_2(\theta_2)$ and since $\alpha_2 \approx 0$, of $I_2(\phi_2)$. Thus the essentially sinusoidal interference pattern in Fig. 11 may be regarded as a direct measurement of the supercurrent-phase relation of the Josephson tunnel junction.

In Figs. 12–14, we show the $I_c(B)$ for a second interferometer of dimensions $A = 0.39 \pm 0.01$ mm, $b = 0.38 \pm 0.01$ mm, $w = 0.35 \pm 0.01$ mm, $l = 4.18 \pm 0.03$ mm, $t_1 = 1700 \pm 150$ Å, $t_2 = 1500 \pm 100$ Å, and $t_{Ge} = 2000 \pm 150$ Å. These data are taken at three successively lower temperatures below the T_c of Sn. The variation in I_{c1} and I_{c2} with T causes the patterns to change from a type-A case in Fig. 12 similar to that of Fig. 4 to a type-B case in Figs. 13 and 14 similar to the case of Fig. 5.

In Fig. 12, taken at $T = 3.71$ °K, the $I_c(B)$ is in a type-A regime as in the previous example, but in this case the pattern is skewed with the value of $\Delta\theta_x$ differing substantially from π, indicating a value of α_2 rather larger than for the junction of

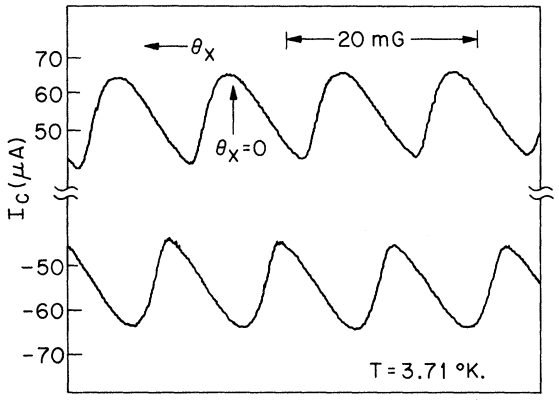

FIG. 12. Positive and negative $I_c(B)$ for a Sn-Sn double junction near T_c. The position of $\theta_x=0$ is deduced in text.

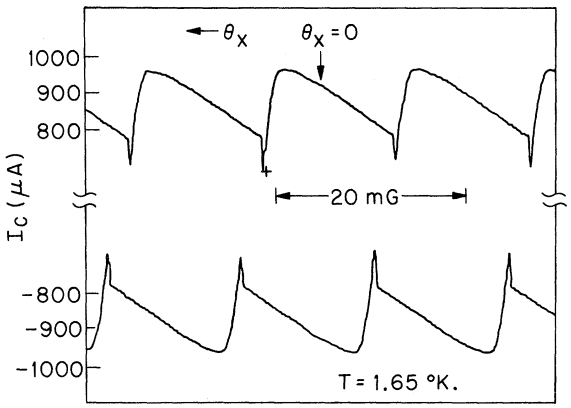

FIG. 14. Positive and negative $I_c(B)$ for the junction of Figs. 12 and 13 at a low temperature. The cross shows the depth of the $I_c(B)$ discontinuity calculated from a zero-damping model.

Fig. 11. From the asymmetry of the slope the direction of increasing θ_x is to the left. The parameters may be extracted as before with the resulting values $I_{c1}=53.5\pm0.7$ μA, $I_{c2}=11.9\pm0.2$ μA, $\alpha_1=(0.052\pm0.025)\pi$, and $\alpha_2=(0.173\pm0.01)\pi$ giving $L_1=0.9\pm0.3\times10^{-12}$ H and $L_2=14.8\pm1.0\times10^{-12}$ H, so that $L=15.7\pm1.3\times10^{-12}$ H. Here use is made of the condition $I_{c2}/(1-\alpha_2)<I_{c1}/(1+\alpha_1)$ in order to reject all but one of the possible values of α_1 which could give rise to the observed $\delta\theta_x$. We note that $I_{c2}/I_{c1}=0.22\pm0.005$ and $\alpha=0.55\pm0.03$, values which from Fig. 3 are consistent with the type-A regime, although they lie near the limit of this regime, a fact reflected by the "pinched" appearance of the minima.

The magnetic field period here is $\Delta B=12.75\pm0.1$ mG, giving a magnetic area $\bar{A}=1.62\pm0.015\times10^{-5}$ cm^2. In this temperature range the penetration depths are not small compared to the film thicknesses and we must use the general forms for $\bar{A}$, Eq. (22) and for L, Eq. (24).

In this case the values $\lambda_1=\lambda_2=2300$ Å give $L=15.7\pm1.1\times10^{-12}$ H and $\bar{A}=1.55\pm0.11\times10^{-5}$ cm^2, in fair agreement with the measured values. The uncertainties given reflect the film thickness uncertainties. Here $\bar{A}$ has almost reached its limiting value and is not very sensitive to the value of λ. The variation in λ which could still give agreement with L and $\bar{A}$ is of order ± 300 Å. This value of λ is reasonable for $t\approx0.99$ but since the transition temperatures of the two films differ by the order of 0.04° the value should not be regarded as a precise determination of λ.

Figure 13 shows the $I_c(B)$ for this double junction at $T=3.19$ °K. Here again the pattern is oscillatory, with smoothly rounded maxima, but the minima consist of two intersecting segments of differing slope. On one side $I_c(B)$ is approaching a rounded minimum, nearly attaining zero slope and on the other side it is descending fairly steeply, giving the cusplike minimum. The presence of the cusp indicates that we have passed out of the type-A regime of Fig. 3 and have entered the regime in which $I_s(\theta_1, \theta_x)$ possess a double maximum for an interval of θ_x about $\theta_x=\pi$. The inset of Fig. 13 shows an expanded view of the cusp, revealing that there is actually a small discontinuity between the two intersecting segments of $I_c(B)$. This indicates, as described in Sec. III, that the jump from the lower of the two maxima of $I_{s1}(\theta_1, \theta_x)$, correspond-

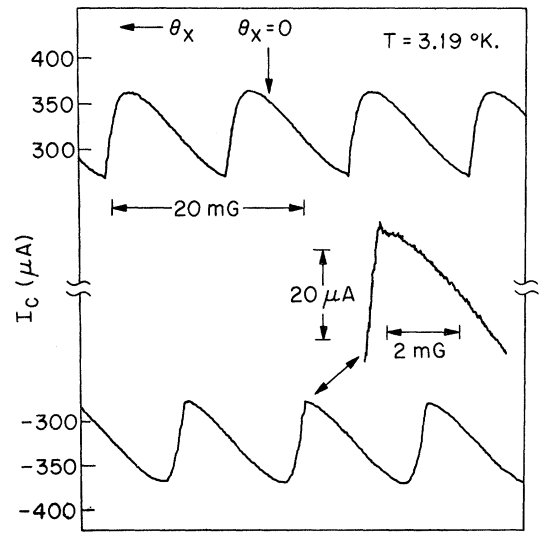

FIG. 13. Positive and negative $I_c(B)$ for the junction of Fig. 12 at a lower temperature. The expanded inset shows the appearance of the minimum, including the slight discontinuity due to the dynamic effects.

ing to the smaller I_c, is unstable in this region. Since the cusp in this case apparently only just obscures the minimum to which the right-hand segment of $I_c(B)$ is tending, it is possible to obtain by extrapolation the position $\Delta\theta_x$ and the depth (ΔI) of this minimum. One can then determine as before the parameters $I_{c1} = 321.3 \pm 1$ μA, $I_{c2} = 44.7 \pm 1$ μA, $\alpha_1 = (0.056 \pm 0.026)\pi$, and $\alpha_2 = (0.318 \pm 0.01)\pi$, and consequently $L_1 = 0.2 \pm 0.1 \times 10^{-12}$ H and $L_2 = 7.24 \pm 0.3 \times 10^{-12}$ H or $L = 7.44 \pm 0.4 \times 10^{-12}$ H. From these values we obtain $\alpha = 1.04 \pm 0.03$ and $I_{c2}/I_{c1} = 0.14$ which from Fig. 3 indicates that the $I_c(B)$ should lie in the type-B regime and just beyond the point at which the minimum changes from rounded to cusplike. The uncertainty in the various α here precludes accurate calculations of the expected size of the discontinuity at minimum. One can explain why it is that the steeply descending segment of $I_c(B)$ extends below the shallow, rather than vice versa. The argument will be given in the next example along with a calculation of the size of the jump.

The magnetic field period ΔB is 13.75 ± 0.1 mG giving $\bar{A} = 1.505 \pm 0.01 \times 10^{-5}$ cm^2. Using the known dimensions along with $\lambda = 1200$ Å we compute from (22) and (24) $\bar{A} = 1.49 \pm 0.1 \times 10^{-5}$ cm^2, $L = 7.6 \pm 0.4 \times 10^{-12}$ H, in reasonable accord with the measured values. The uncertainty in λ is about ± 150 Å. At this reduced temperature $t = 0.85$ we expect $\lambda = 1.45\,\lambda(t=0)$ which would make $\lambda(t=0) \approx 850 \pm 100$ Å. This is in fact close to the observed low-temperature value as we shall see.

In Fig. 14, we show the $I_c(B)$ of this junction at $T = 1.65$ °K. The $I_c(B)$ shows oscillations with rounded maxima but having minima possessing a discontinuous transition between two segments of $I_c(B)$. The segments approach each other as if to form a cusplike minimum, but because of the dynamics the lower jump is unstable. We defer for the moment consideration of the dynamics and concentrate on the shape of $I_c(B)$. In this case the smooth minimum of the $I_c(B)$ is concealed, with neither its position nor its depth being obvious from the $I_c(B)$ alone, although by extrapolation from the previous higher-temperature curves it must lie somewhat to the right of the observed minimum. Consequently we cannot directly determine the separate values of I_{c1}, I_{c2}, α, and α_2 in the manner used for the previous cases. It is feasible, however, to extrapolate the higher-temperature values and make an approximate determination of these quantities. We note first of all that the maximum I_c is 954 ± 3 μA. If we extrapolate the ratio I_{c2}/I_{c1} from the previous measurements [making use also of another set of $I_c(B)$, not shown here, which were taken at a temperature of 2.86 °K] we conclude that $I_{c2}/I_{c1} = 0.11 \pm 0.01$ is a reasonable extrapolation and thus we obtain that $I_{c1} = 849 \pm 10$ μA and $I_{c2} = 105 \pm 10$ μA. Now the portion of $I_c(B)$ to the left-hand side of each minimum in Fig. 14 corresponds to the portions of $I_c(B)$ on the left-hand side of the minima in Figs. 12 and 13. In Fig. 14, the slope of this portion clearly reaches a maximum before the curve terminates in the discontinuity. The magnitude of this maximum slope is $I_{c2}/(1+\alpha_2)$, and is 40.2 ± 2 μA/rad, giving $\alpha_2 = (0.5 \pm 0.12)\pi$. The value of $\delta\theta_x/2\pi = \alpha_2/\pi - \alpha_1/\pi$ is $n + 0.552 \pm 0.04$, where n is some integer. Noting the small values of L_1 at the higher temperature we conclude that $n = 0$ and $\alpha_1 = (0 \pm 0.15)\pi$, $L_1 = 0.0 \pm 0.2 \times 10^{-12}$ H and $L_2 = 5.3 \pm 0.6 \times 10^{-12}$ H. Note that the value of $\alpha = 1.57 \pm 0.37$ and $I_{c2}/I_{c1} = 0.11$ is in accord with the cusplike nature of the minimum according to Fig. 3.

From the magnetic period $\Delta B = 15.35 \pm 0.1$ mG we obtain $\bar{A} = 1.345 \pm 0.01 \times 10^{-5}$ cm^2. If we take $\lambda = 700$ Å we obtain $\bar{A} = 0.37 \pm 0.1 \times 10^{-5}$ cm^2 and $L = 5.4 \pm 0.4 \times 10^{-12}$ H from Eqs. (22) and (24). This value of λ has an uncertainty of about ± 100 Å and is again larger than that usually proposed for Sn, which may be due to mean-free-path effects.

The discontinuous jump at the minimum of $I_c(B)$ in this example is caused by the dynamics. We shall now consider three aspects of the jump. The first point is to explain why it is that the steeper of the two intersecting segments is observed below the extrapolated point of intersection rather than the shallower. Recalling the values of α_1 and α_2, we observe that the $I_1(\theta_1)$ is basically a sinusoid while the smaller amplitude $I_2(\theta_2)$ is a reentrant function, having an ascending slope which is relatively gentle and a descending slope which becomes infinitely steep just beyond the maximum. As θ_x is increased from $\alpha_2 - \alpha_1$, the peak of $I_{c+}(\theta_x)$, a double maximum of $I_s(\theta_1, \theta_x)$ is formed which roughly corresponds to the sharp maximum of I_2 moving down the steep side of $I_1(\theta_1)$ and the peak of I_1 superimposed on and moving up the gentle slope of I_2. The former peak, which corresponds to the steep descent of $I_{c+}(\theta_x)$, occurs at the smaller value of θ_1 and is the first maximum encountered on $I_s(\theta_1, \theta_x)$ as I_t is increased from zero. Thus it is from this point that the jump occurs, and if the jump is unstable then the observed $I_{c+}(\theta_x)$ will correspond to the steep segment of $I_{c+}(\theta_x)$ even though the segment of shallow slope may have a larger magnitude.

The second point involves the absolute magnitude of the jump. Using the considerations set forth in Appendix B we can calculate the point at which the jump would turn from stable into unstable, assuming no damping. Such a calculation really requires that one know the four parameters α_1, α_2, I_{c1}, and I_{c2} precisely. Since our knowledge of these is somewhat rough we take the easier course of approximating $I_1(\theta_1)$ by the sinusoid

$I_1(\theta_1) = I_{c1} \sin\theta_1$ for $I_{c1} = 850$ μA and $I_2(\theta_2)$ by the sawtooth $I_2(\theta_2) = I_{c2}(\theta_2/\pi)$, where $I_{c2} = 105$ μA. The sawtooth terminates at $\theta_2 = \pm\pi$. From these one can calculate that the point at which the steep branch of $I_{c+}(\theta_x)$ becomes stable is at $\theta_x \approx \alpha_2 - \alpha_1 + 0.83$ and $I_{c+} \approx 674$ μA, the point indicated by the cross in Fig. 15.

The third point concerning the dynamics is to note that, according to Appendix B, for zero damping the lowest value of $I_{c+}(\theta_x)$ on the metastable branch is independent of the value of $L_1 - L_2$ and depends only on L. In Fig. 15, we show the $I_c(B)$ for this interferometer which is observed when one changes the current lead from one end of the cross strip to the other. As can be seen by comparison with Fig. 15, this criterion is very nearly satisfied.

Finally, in Fig. 16, we show the $I_c(B)$ measured at $T = 3.08$ °K for a third double junction of dimensions $A = 0.30 \pm 0.01$ mm, $b = 0.05 \pm 0.007$ mm, $l = 3.15 \pm 0.02$ mm, $w = 0.20 \pm 0.005$ mm, $t_1 = 2500 \pm 200$ Å, $t_2 = 2800 \pm 200$ Å, and $t_{Ge} = 9300 \pm 300$ Å. This junction shows the phenomenon of multiple critical currents[20] characteristic of the regime which is exemplified in Fig. 7. In each cycle of the ac current bias the junction switches from $V = 0$ to $V \neq 0$ at any of three or four discrete values whose magnitude depends on B. The choice of which is observed as the critical current is apparently random with different probabilities for each value. The dependence of these different I_c's on B is displayed in Fig. 16 which shows that they depend on B in an identical fashion with a fixed phase shift which is just the magnetic field period $\Delta B = 5.70 \pm 0.30$ mG corresponding to $\Delta\theta_x = 2\pi$.

For the moment we concentrate on attempting to interpret the shape of a single branch of $I_c(B)$. This consists of an essentially linear portion at the right, reaching a peak at 622 ± 6 μA at, say,

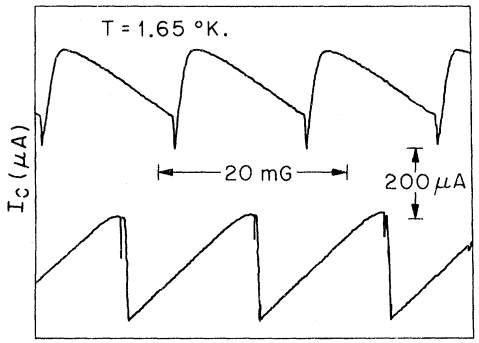

FIG. 15. Positive $I_c(B)$ for the junction of Figs. 12–14. The upper curve repeats the data of Fig. 14, while the lower shows the effect of changing the current input in the other end of the cross strip.

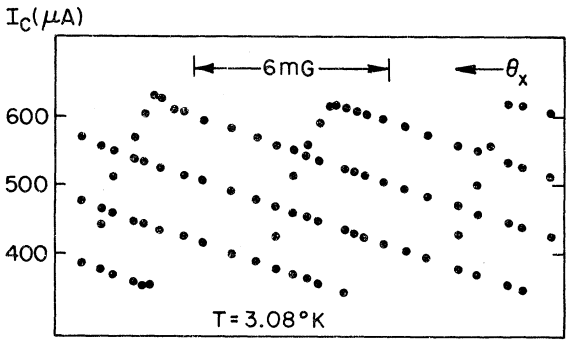

FIG. 16. Positive $I_c(B)$ for a Sn-Sn double junction showing multiple critical currents.

$\theta_x = 0$ and extending down to a current of 350 ± 10 μA at a value of $\theta_x = (6.0 \pm 0.1)\pi$, giving a slope of 14.4 ± 0.3 μA/rad. The segment of $I_c(B)$ to the left of the maximum, on the other hand, is noticeably curved, particularly near the maximum, and descends much more steeply. The maximum slope of this portion is $dI_c/d\theta_x = 110 \pm 15$ μA/rad, and the segment terminates (i.e., the corresponding I_c no longer is observed) at $\Delta\theta_x = -(0.65 \pm 0.05)\pi$ from the maximum and at $I_c = 420 \pm 10$ μA.

In a case such as this, in which the value of α is obviously larger than in the previous example, there is no sure means of determining the individual values of I_{c1}, I_{c2}, α_1, and α_2, but certain conclusions can be drawn. We first note that the area of the two junctions differs by a factor of 6, so that it may be assumed that the smaller junction corresponds to I_{c2}. As it happens this was the junction on the side of the interferometer having the current lead on the cross strip, so that most probably the inequalities $L_1 \gg L_2$ and $\alpha_1 \gg \alpha_2$ apply. Thus $I_1(\theta_1)$ will probably be a highly reentrant function, being nearly linear over most of the region corresponding to $-\frac{1}{2}\pi - \alpha_1 < \theta_1 < \frac{1}{2}\pi + \alpha_1$ and going suddenly to a negatively infinite slope just beyond these points. Under these conditions it turns out that on one side of its maximum $I_c(\theta_x)$ reproduces rather closely the shape of $I_2(\theta_2)$, since the value of θ_1 is held nearly fixed by the steepness of $dI_1/d\theta_1$ in this area. On the other side of the maximum of $I_c(\theta_x)$ the reverse situation generally holds. Provided that $I_{c2}/I_{c1} + \alpha \gg 1$ the slope of $dI_1/d\theta_1$ at I_c is small compared to the slope of $dI_2/d\theta_2$. We associate the linear segment of $I_c(B)$ on the right-hand side of the maximum in Fig. 17 with the presumed near-linear $I_1(\theta_1)$ and the nonlinear segment on the left of the maximum with $I_2(\theta_2)$. The slope 14.4 μA/rad of the linear segment should then give a measure of $I_{c1}/1 + \alpha_1$. Since $I_{c1} \gtrapprox 311$ μA the value of α_1 must be $\alpha_1 \gtrapprox 20$, and the slope of $I_1(\theta_1)$ should be approximately given by I_{c1}/α_1

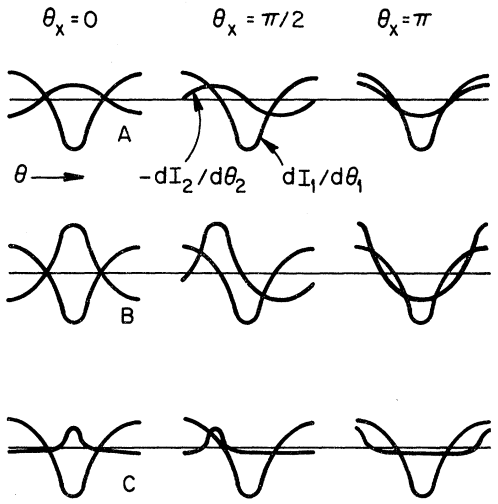

FIG. 17. Derivatives of $I_1(\theta_1)$ and $I_2(\theta_1+\theta_x)$ in three schematic cases. The value of θ_x increases from 0 to π from left to right. The intersections of the curves are the extrema of $I_s(\theta_1, \theta_x)$.

$= \Phi_0/2\pi L_1$, giving $L_1 = 22.9 \pm 0.5 \times 10^{-12}$ H.

From the nonlinear shape of the left-hand segment of $I_c(B)$ it is apparent that the value of α_2 is not large compared to unity. We can roughly estimate the values of I_{c2} and α_2. There is an upper bound of 310 μA on I_{c2}, and, since the $I_c(B)$ segment seems to terminate without reaching a maximum slope, a lower bound of 200 μA. We then have 200 $\mu A < I_{c2} < 310$ μA, and from the shape we can estimate $0 \lesssim \alpha_2 \lesssim 1.5$. The complete list of parameters is then 200 $\mu A < I_{c2} < 310$ $\mu A < I_{c1} < 420$ μA, $0 < \alpha_2 < 1.5$ and $20 < \alpha_1 < 30$. We can also obtain $L_2 \lesssim 3 \times 10^{-12}$ H and with somewhat more accuracy $L_1 = 22.9 \pm 0.5 \times 10^{-12}$ H, for a total $L = 24.4 \pm 2.0 \times 10^{-12}$ H.

In this case ΔB was less accurately known, being 5.70 ± 0.3 mG, giving $\bar{A} = 3.64 \pm 0.2 \times 10^{-5}$ cm^2. The bulk of this area is due to the Ge. At this temperature we estimate the value of $\lambda = 1.35\lambda(T=0)$, so that $\lambda \approx 700$ Å if $\lambda(T=0) = 510$ Å, the generally accepted value for pure Sn. Short-mean-free-path effects could increase this value. If we take $\lambda = 800 \pm 100$ Å we obtain, using (22) and (24), $\bar{A} = 3.48 \pm 0.15 \times 10^{-5}$ cm^2 and $L = 21.8 \pm 1.2 \times 10^{-12}$ H.

In summary, we have discussed the quantum interference properties of double weak-link junctions, with emphasis on the dependence of the critical current I_c on applied magnetic field B. The model employed takes account of the dependence on the individual critical currents and the self-magnetic field screening (including both self-inductance and asymmetry). It also includes the dynamic effects (both adiabatic and nonadiabatic changes of the phases in response to applied current) legislated by the capacitance and dissipative processes. The resulting nonlinear equations can be treated by a simple graphical approach. This analysis, with the conceptual aid of a mechanical analog (the double pendulum) appears to provide a complete qualitative understanding of the diverse behavior of $I_c(B)$ in such junctions, and allows a quantitative analysis of experimental $I_c(B)$ in many cases. The predictions of the model are illustrated by the experimental $I_c(B)$ of Sn-Sn tunnel junctions over a range of critical currents and magnetic geometries. The junctions show behavior [discontinuous and multiple-valued $I_c(B)$] which demonstrates the role of the dynamics.

The understanding of "classical" Josephson effects as predicted by the simplest equations is desirable not only in its own right but also as a necessary condition for the study of more subtle properties such as fluctuations or quantum effects. The fact that one can understand the basic behavior of $I_c(B)$ of double junctions by these relatively simple means should allow them to be used effectively in such studies.

ACKNOWLEDGMENTS

We would like to thank D. B. Sullivan and J. E. Zimmerman for suggesting the usefulness of a mechanical analog in a conversation (Ref. 22) and Mrs. R. C. Fulton for the computer calculations.

APPENDIX A

In this Appendix we derive some of the results involved in the analysis of Sec. II. We first demonstrate that $\alpha = \alpha_2 + (I_{c2}/I_{c1})\,\alpha_1$ is a more important parameter than α_1 or α_2. The constraint (5) can be written

$$\phi_2 - \phi_1 = \theta_x + 2\pi L_1 I_1(\phi_1)/\Phi_0 - 2\pi L_2 I_2(\phi_2)/\Phi_0 \,. \tag{A1}$$

If we define the loop current $I_R = \frac{1}{2}[I_1(\phi_1) - I_2(\phi_2)]$ then (A1) becomes

$$\phi_2 - \phi_1 = \theta_x + 2\pi L I_R/\Phi_0 + \pi(L_1 - L_2) I_t/\Phi_0 \,. \tag{A2}$$

Suppose now L_1 and L_2 are fixed and I_t and θ_x have the particular values $\bar{\theta}_x$ and $\bar{I}_t$, causing ϕ_2 and ϕ_1 to take on the particular values $\bar{\phi}_2$ and $\bar{\phi}_1$. If we then decrease L_2 and increase L_1 by equal amounts ΔL (easily done experimentally), leaving L fixed, by also adjusting θ_x to the new value $\theta_x = \bar{\theta}_x - 2\pi \Delta L \bar{I}_t/\Phi_0$ we again arrive at the same values $\phi_1 = \bar{\phi}_1$ and $\phi_2 = \bar{\phi}_2$ as satisfying both the constraint and $I_t = \bar{I}_t$. The implication of this is that the new problem with different L_1 and L_2 is in complete correspondence to the original one once θ_x is replaced by $\theta_x - 2\pi \Delta L I_t/\Phi_0$. Since α is proportional to $L = L_1 + L_2$, the effect on $I_c(\theta_x)$ of changing α_1 and α_2 while leaving α and I_{c2}/I_{c1} fixed is merely to introduce a displacement in the value of θ_x corre-

sponding to a given I_c, the displacement being proportional to I_c.[21] The maximum and minimum values of I_c remain unchanged as do qualitative features such as cusplike minima or breaks in slope. This shows why regimes *A*, *B*, and *C* involve only α and I_{c2}/I_{c1}. [If ΔL is large enough that either L_2 or L_1 becomes negative then the $I_c(\theta_x)$ must become reentrant and therefore multivalued. We will not go into these complications, however.]

We next consider the shapes of $I_c(\theta_x)$ in the various regimes, specializing to sinusoidal $I(\phi)$. Given that

$$\theta_1 = \phi_1 + \alpha_1 \sin\phi_1 , \tag{A3}$$

$$\theta_2 = \phi_2 + \alpha_2 \sin\phi_2 , \tag{A4}$$

it follows that

$$\frac{d\phi_1}{d\theta_1} = (1 + \alpha_1 \cos\phi_1)^{-1} , \tag{A5}$$

$$\frac{d^2\phi_1}{d\theta_1^2} = -\alpha_1 \sin\phi_1 (1 + \alpha_1 \cos\phi_1)^{-3} , \tag{A6}$$

$$\frac{dI_1}{d\theta_1} = \frac{I_{c1}}{\alpha_1}\left(1 - \frac{d\phi_1}{d\theta_1}\right) = I_{c1}\cos\phi_1 (1 + \alpha_1 \cos\phi_1)^{-1} , \tag{A7}$$

$$\frac{d^2I_1}{d\theta_1^2} = \frac{I_{c1}}{\alpha_1}\frac{d^2\phi_1}{d\theta_1^2} = -I_{c1}\sin\phi_1 (1 + \alpha_1 \cos\phi_1)^{-3} , \tag{A8}$$

with similar relations between I_2, ϕ_2, and θ_2. The net transport current I_t is

$$I_t = I_1(\theta_1) + I_2(\theta_1 + \theta_x) = I_s(\theta_1, \theta_x) . \tag{A9}$$

The extrema of $I_s(\theta_1, \theta_x)$, both primary and secondary, occur at the points $dI_s/d\theta_1 = 0$, or at those θ_1, call them θ_1', such that

$$\left(\frac{dI_1(\theta_1)}{d\theta_1}\right)_{\theta_1 = \theta_1'} = \left(-\frac{dI_2(\theta_2)}{d\theta_2}\right)_{\theta_2 = \theta_1' + \theta_x} . \tag{A10}$$

A convenient graphical approach to thinking about the properties of $I_c(\theta_x)$ is to plot $dI_1/d\theta_1$ and $-dI_2/d\theta_2$ and overlap them with a phase lag θ_x. The intersections of the two then occur at the extrema of $I_s(\theta_1, \theta_x)$. We show three examples of this approach in Fig. 17, in which three examples from regimes *A*, *B*, and *C* have been plotted for various representative θ_x. These plots show clearly how the three regimes differ. In case *A* for all θ_x there are always only two intersections, corresponding to $I_{c+}(\theta_x)$ and $I_{c-}(\theta_x)$. The right-left symmetry of the derivatives reflects the time-reversal requirements, $I_{c+}(+\theta_x) = -I_{c-}(-\theta_x)$. The fact that the value of θ_1, at the intersection corresponding to I_{c+} (say, θ_1') varies smoothly and periodically with θ_x leads to the conclusion that $I_{c+}(\theta_x)$ is also a smooth periodic function. We can compute the slope of $I_{c+}(\theta_x)$ by noting that $I_{c+}(\theta_x) = I_s[\theta_1'(\theta_x), \theta_x]$ so that

$$\frac{dI_{c+}}{d\theta_x} = \left(\frac{dI_1}{d\theta_1}\right)_{\theta_1 = \theta_1'}\frac{d\theta_1'}{d\theta_x} + \left(\frac{dI_2}{d\theta_2}\right)_{\theta_2 = \theta_1' + \theta_x}\left(\frac{d\theta_1'}{d\theta_x} + 1\right) , \tag{A11}$$

and taking account of (A10) this becomes

$$\frac{dI_{c+}}{d\theta_x} = \left(\frac{dI_2}{d\theta_2}\right)_{\theta_2 = \theta_1' + \theta_x} = -\left(\frac{dI_1}{d\theta_1}\right)_{\theta_1 = \theta_1'} . \tag{A12}$$

Thus the slopes $dI_c/d\theta_x$ and $dI_2/d\theta_2$ have a point-by-point correspondence. Since θ_1' is bounded, as θ_x increases through 2π so does $\theta_2 = \theta_1' + \theta_x$, so that a plot of $dI_c/d\theta_x$ over a cycle is in effect a complete plot of $dI_2/d\theta_2$ over a cycle, except that the relation between θ_2 and θ_x is nonlinear. It follows that the maximum and minimum of I_{c+}, which occur at $dI_{c+}/d\theta_x = 0$, correspond to the points at which $dI_2/d\theta_2 = 0$, or at $[I_{c+} = I_{c1} + I_{c2},\ \theta_x = \alpha_2 - \alpha_1]$ and $[I_{c+} = I_{c1} - I_{c2},\ \theta_x = \pi - (\alpha_1 + \alpha_2)]$, respectively. It also follows that the maximum and minimum slope of $I_{c+}(\theta_x)$ are $\pm I_{c2}/(1 \pm \alpha_2)$.

In addition, we note any particular value of $dI_{c+}/d\theta_x$ (other than the extremes), say, $(dI_{c+}/d\theta_x)'$ occurs twice in a cycle of θ_x, say, at θ_x' and θ_x''. But the values of $\theta_1'(\theta_x')$ and $\theta_1'(\theta_x'')$ are the same because $-(dI_1/d\theta_1)_{\theta_1 = \theta_1'} = (dI_{c+}/d\theta_x)'$ in both cases. Consequently the values of $\theta_2 = \theta_1' + \theta_x$ at $\theta_x = \theta_x'$ and θ_x'' differ by exactly the observed value $\theta_x'' - \theta_x'$. Hence by plotting $dI_{c+}/d\theta_x$ vs θ_x and extracting from it $(dI_{c+}/d\theta_x)'$ vs $\theta_x'' - \theta_x'$ for all the values of $(dI_{c+}/d\theta_x)'$ from $I_{c2}/(1 + \alpha_2)$ to $-I_{c2}/(1 - \alpha_2)$ we create a plot of $dI_2/d\theta_2$ vs θ_2 which can then be integrated to give $I_2(\theta_2)$. This is the approach mentioned in Sec. II. We note here incidentally that the second derivative $d^2I_c/d\theta_x^2$ is given by

$$\frac{d^2I_c}{d\theta_x^2} = \left[\left(\frac{d^2I_1}{d\theta_1^2}\right)^{-1}_{\theta_1 = \theta_1'} + \left(\frac{d^2I_2}{d\theta_2^2}\right)^{-1}_{\theta_2 = \theta_1' + \theta_{x1}}\right]^{-1} . \tag{A13}$$

In the example of type *B* in Fig. 17, it is obvious that $dI_1/d\theta_1$ and $-dI_2/d\theta_2$ have four intersections in a symmetric interval about $\theta_x = \pi$, leading to the double-humped property. Here as well, the rate of change of the heights of these extrema is given by the values of $dI_2/d\theta_2 = -dI_1/d\theta_1$ at the intersections. Consider what happens as $-dI_2/d\theta_2$ is moved from right to left with increasing θ_x, starting at $\theta_x = 0$. This is a condition in which there are only two intersections at θ_1' and θ_1'', corresponding, respectively, to the maximum and minimum of $I_s(\theta_1, \theta_x)$. As θ_x increases there comes a point, say at $\tilde{\theta}_x$, at which $-dI_2/d\theta_2$ and $dI_1/d\theta_1$ touch, forming a second pair of points of intersection, θ_1''' and θ_1''''. These correspond, respectively, to a minimum and maximum. At $\tilde{\theta}_x$, $\theta_1''' = \theta_1''''$, and $I_s(\theta_1''', \tilde{\theta}_x) = I_s(\theta_1'''', \tilde{\theta}_x) < I_s(\theta_1', \theta_x)$ but as θ_x increases they pull apart, and $I_s(\theta_1''', \theta_x) < I_s(\theta_1'''', \theta_x)$ for all θ_x. Now at $\theta_x = 2\pi - \tilde{\theta}_x$ a precisely symmetric situation occurs with two intersections coming back together and disappearing.

If one follows the progress of the intersections for θ_x lying between these values, however, it can be seen that the intersections which come together at $\theta_x = 2\pi - \tilde{\theta}_x$ are θ_1' and θ_1''. From the symmetry of this case with $\theta_x = \tilde{\theta}_x$ it follows that the values of $I_s(\theta_1', 2\pi - \tilde{\theta}_x) = I_s(\theta_1'', 2\pi - \tilde{\theta}_x)$ must lie between the values of $I_s(\theta_1'', 2\pi - \tilde{\theta}_x)$ and $I_s(\theta_1'', \tilde{\theta}_x)$ so that somewhere between $\theta_x = \tilde{\theta}_x$ and $\theta_x = 2\pi - \tilde{\theta}_x$ the values of $I_s(\theta_1', \theta_x)$ and $I_s(\theta_1'', \theta_x)$, the two maxima, must be equal as was asserted in Sec. II. This point corresponds to the break in slope or cusplike minimum of $I_{c+}(\theta_x)$. Further, since $\theta_1' \neq \theta_1''$ at this point, the rates of change of the two maxima with θ_x, which are given by $-(dI_1/d\theta_1)_{\theta_1=\theta_1'}$ and $-(dI_1/d\theta_1)_{\theta_1=\theta_1''}$, are different, as claimed in Sec. II.

In the type-C example of Fig. 17 we see that the regions of θ_x for which there are four intersections occupy two limited, symmetric sections of θ_x on either side of $\theta_x = \pi$ but not including that point. Consideration of the appearance and disappearance of the intersections with increasing θ_x leads to the same conclusions as in the type-B case regarding the existence of the break in slope. We will present here the criteria which lead to the distinction between type-A and type-C cases. In this we take advantage of the fact that in the latter case for some θ_x there will be a transition between a four-intersection situation and one of two intersections. At this point an intermediate maximum and minimum of $I_s(\theta_1, \theta_x)$ have just come together so that both the first and second derivatives of $I_s(\theta_1, \theta_x)$ with respect to θ_1 vanish at one point. The boundary between A and C can then be determined by evaluating $d^2I_s/d\theta_1^2$ at the points at which $dI_s/d\theta_1$ vanishes for various combinations of α and I_{c2}/I_{c1} and finding whether $d^2I_s/d\theta_1^2$ vanishes for any θ_x. If so, the case is type C, if not, type A. To do this we note that at a maximum or minimum ϕ_2 and ϕ_1 are related by

$$I_{c1}\cos\phi_1\,(1+\alpha_1\cos\phi_1)^{-1} = -I_{c2}\cos\phi_2 \times (1+\alpha_2\cos\phi_2)^{-1} \quad \text{(A14)}$$

or

$$(I_{c2}/I_{c1})\,(\cos\phi_1)^{-1} = -(\cos\phi_2)^{-1} - \alpha\,. \quad \text{(A15)}$$

The second derivative [using (A8)] is

$$\frac{d^2I_s}{d\theta_1^2} = -I_{c1}\sin\phi_1\,(1+\alpha_1\cos\phi_1)^{-3} - I_{c2}\sin\phi_2\,(1+\alpha_2\cos\phi_2)^{-3}\,, \quad \text{(A16)}$$

where ϕ_2 and ϕ_1 at the maximum are related by (A15). We can therefore write $d^2I_s/d\theta_1^2$ at any extrema as

$$\left(\frac{d^2I_s}{d\theta_1^2}\right)_{\max} = (1+\alpha_2\cos\phi_2)^{-3} \times \left[I_{c1}\sin\phi_1\left(\frac{I_{c2}\cos\phi_2}{I_{c1}\cos\phi_1}\right)^3 - I_{c2}\sin\phi_2\right], \quad \text{(A17)}$$

which is only zero if

$$I_{c1}\sin\phi_1(I_{c1}\cos\phi_1)^{-3} = I_{c2}\sin\phi_2(I_{c2}\cos\phi_2)^{-3}\,. \quad \text{(A18)}$$

Squaring both sides and employing (A15) again we arrive at the requirement

$$(I_{c2}/I_{c1})^{-2}\,[-(\cos\phi_1)^{-1} - \alpha]^6 - [-(\cos\phi_1)^{-1} - \alpha]^4 - (\cos\phi_1)^{-6} + (\cos\phi_1)^{-4} = 0\,, \quad \text{(A19)}$$

which is polynomial in $(\cos\phi_1)^{-1}$ and must possess zeros for some value of $\cos\phi_1$ if $d^2I_s/d\theta_1^2$ vanishes at the maximum, and vice versa. The boundary between A and C in Fig. 3 is determined by numerically investigating the value of the polynomial between $0 < \cos\phi_1 < 1$ for various fixed I_{c2}/I_{c1} and α. The task is relatively easy because the polynomial possesses only a single well-defined minimum.

Finally, we justify the assertion of Sec. III that in regime C there is only one stable state at $I_t = 0$. Recall the situation in the C regime (Fig. 17). At $\theta_x = \alpha_2 - \alpha_1$ the $dI_1/d\theta_1$ and $-dI_2/d\theta_2$ intersect at zero corresponding to $I_{c+} = I_{c1} + I_{c2}$. As θ_x increases this maximum of $I_s(\theta_1, \theta_x)$ whose position we shall call θ_1' decreases at a rate $dI_{c+}/d\theta_x = (-dI_1/d\theta_1)_{\theta_1=\theta_1'}$ which for $\alpha_2 - \alpha_1 < \theta_x < \pi$ is always negative, while as θ_x increases at some point the new maximum and minimum form at a larger θ_1 and smaller $I_s(\theta_1, \theta_x)$. This secondary minimum whose position we call θ_1'', is always below the original maximum at θ_1' but decreases at a slower rate, because $(-dI_1/d\theta_1)_{\theta_1=\theta_1'} < (-dI_1/d\theta_1)_{\theta_1=\theta_1''}$. Ultimately at a value $\theta_x = \theta_{xf} < \pi$ the original maximum and new minimum combine and disappear at some point $\theta_1 = \theta_{1f}$, where $\theta_{1f} > 0$. Now if the minimum at θ_1'' had ever become negative in this process the maximum at θ_1' would also, because the two ultimately came to the same value and both decrease monotonically with θ_x in this range. But this cannot be the case because the value of $I_s(\theta_1', \theta_x)$ at the point where the $\theta_1' = \theta_1''$ must be given by

$$I_{c1} + I_{c2} - \int_{\alpha_2-\alpha_1}^{\theta_{xf}} \left(\frac{dI_1}{d\theta_1}\right)_{\theta_1=\theta_1'} d\theta_x$$

or

$$I_{c1} + I_{c2} - \int_{\pi/2}^{\theta_{1f}} \frac{dI_1}{d\theta_1}\left(\frac{d\theta_x}{d\theta_1}\right)_{\theta_1=\theta_1'} d\theta_1\,,$$

and since $\theta_{1f} > 0$ and $|d\theta_x/d\theta_1| < 1$ (as can be seen from the Fig. 17), the integral is less than I_{c1}. Consequently, $I_s(\theta_{1f}, \theta_x) > 0$ and the minimum can never pass through zero.

APPENDIX B

In this Appendix we discuss the energetics of the double junction and double pendulum. The discussion is in the notation of Fig. 8(b). We assume that no dissipation occurs and that both the

external flux $\Phi_x = \theta_x \Phi_0/2\pi$ and the current bias I_t are fixed. Then the energy of the system can be written

$$E = \tfrac{1}{2}C_1 V_1^2 + \tfrac{1}{2}C_2 V_2^2 + \tfrac{1}{2}L_1 I_{j1}^2 + \tfrac{1}{2}L_2 I_{j2}^2 - (\Phi_0/2\pi)(I_{c1}\cos\phi_1 + I_{c2}\cos\phi_2) - (\Phi_0/2\pi) I_t \phi_q \,, \quad \text{(B1)}$$

where $(\Phi_0/2\pi)\phi_q$ is the time-integrated voltage drop V_q around the path between the leads through L_1. Noting that $I_{j1} = (\Phi_0/2\pi)(\phi_q - \phi_1)/L_1$ and $I_{j2} = (\Phi_0/2\pi)(\phi_q + \theta_x - \phi_2)/L_2$ we may rewrite E as

$$E = (\Phi_0/2\pi)^2 [\tfrac{1}{2}C_1 (d\phi_1/dt)^2 + \tfrac{1}{2}C_2 (d\phi_2/dt)^2 + (\phi_q - \phi_1)^2/2L_1 + (\phi_q + \theta_x - \phi_2)^2/2L_2 - (2\pi/\Phi_0)((I_{c1}\cos\phi_1 + 1_{c2}\cos\phi_2) + I_t\phi_q)] \,. \quad \text{(B2)}$$

The first two terms we may call the kinetic energy T and the others the potential energy V. In a stationary state we would have both $d\phi_1/dt = d\phi_2/dt = 0$ and $\partial V/\partial\phi_1 = \partial V/\partial\phi_2 = \partial V/\partial\phi_q = 0$. The latter three equations give

$$(\phi_1 - \phi_q)/L_1 + (2\pi/\Phi_0) I_{c1}\sin\phi_1 = 0 \,, \quad \text{(B3)}$$

$$(\phi_2 - \phi_q - \theta_x)/L_2 + (2\pi/\Phi_0) I_{c2}\sin\phi_2 = 0 \,, \quad \text{(B4)}$$

$$(\phi_q - \phi_1)/L_1 + (\phi_q + \theta_x - \phi_2)/L_2 - (2\pi/\Phi_0) I_t = 0 \,. \quad \text{(B5)}$$

These equations, when combined, reproduce the basic double junction equations (1) and (5) along with the additional relation

$$\phi_q = \phi_1 + \alpha_1 \sin\phi_1 = \theta_1 \,. \quad \text{(B6)}$$

Consequently, the energy minima correspond to the stable solutions of the double junction equations, e.g., (11), as one expects.

Consider the function V as it depends upon the three variables ϕ_1, ϕ_2, and ϕ_q. Let ϕ_1', ϕ_2', and ϕ_q' be a point of minimum V.

For type-A situations, we know that this point and the conjugate points $\phi_1' + n2\pi$, $\phi_2' + n2\pi$, and $\phi_q' + n2\pi$, where $n = \pm 1, \pm 2$, etc., are the only minima.

For type-B or type-C situations there may be several minima corresponding to the various stable solutions, each of which has its conjugate points at 2π intervals. In between these minima there are various paths in (ϕ_1, ϕ_2, ϕ_q) space, one of which minimizes the maximum value of V encountered on the path between the two minima. These are the saddle points of V and the energy barrier relevant to Sec. III is the difference in energy between V at these points and at the higher of the two minima.

Now at the saddle points the relations $\partial V/\partial\phi_1 = \partial V/\partial\phi_2 = \partial V/\partial\phi_q = 0$ also apply, which means that these points also correspond to solutions of (11). Since the stable solutions all correspond to minima of V, it is the unstable solutions that correspond to saddle points of V. Some study of Fig. 5 shows that the unstable solutions are in one-to-one correspondence with the stable solutions. That is, between each two neighboring θ_1 corresponding to the latter there is a θ_1 corresponding to the former. This point is the saddle point corresponding to the two minima.

The height of the energy barrier can be computed most easily by noting that at the minima and at the saddle points we can express V in terms of the variables θ_1' and θ_2' which correspond to the ϕ_1' and ϕ_2' at these points. We first rewrite V as

$$V = \tfrac{1}{2}L_1 I_{c1}\sin^2\phi_1' - (\Phi_0/2\pi) I_{c1}\cos\phi_1' + \tfrac{1}{2}L_2 I_{c2}\sin^2\phi_2' - (\Phi_0/2\pi) I_{c2}\cos\phi_2' - (\Phi_0/2\pi) I_t[\phi_1' + (2\pi L_1 I_{c1}/\Phi_0)\sin\phi_1'] \,, \quad \text{(B7)}$$

an expression which is only correct at the minima and saddle points. We can rewrite this in integral form as

$$V = \frac{\Phi_0}{2\pi}\left[\int_0^{\phi_1'} I_{c1}\sin\phi_1 \left(d\phi_1 + \frac{2\pi L_1 I_{c1}}{\Phi_0}\cos\phi_1\, d\phi_1\right) - I_{c1} + \int_0^{\phi_2'} I_{c2}\sin\phi_2 \left(d\phi_2 + \frac{2\pi L_2 I_{c2}}{\Phi_0}\cos\phi_2\, d\phi_2\right) - I_{c2} - I_t\int_0^{\phi_1'}\left(d\phi_1 + \frac{2\pi L_1 I_{c1}}{\Phi_0}\cos\phi_1\, d\phi_1\right)\right]$$

$$= \frac{\Phi_0}{2\pi}\left(\int_0^{\theta_1'} I_1(\theta_1)\, d\theta_1 + \int_0^{\theta_2'} I(\theta_2)\, d\theta_2 - \int_0^{\theta_1'} I_t\, d\theta_1 - (I_{c1} + I_{c2})\right)$$

$$= \frac{\Phi_0}{2\pi}\left(\int_0^{\theta_1'} [I_s(\theta_1, \theta_x) - I_t]\, d\theta_1 + \int_0^{\theta_x} I(\theta_2)\, d\theta_2 - (I_{c1} + I_{c2})\right) \,. \quad \text{(B8)}$$

The latter integral is constant and can be ignored. Its appearance here can be traced to the fact that we have left out any energy factors involved in changes of θ_x. The former term is just the difference between the areas under $I_s(\theta_1, \theta_x)$ and I_t as described in Sec. III. Thus if θ_1' is a minimum and θ_1'' a saddle point the energy barrier between θ_1' and the subsequent minimum is just $(\Phi_0/2\pi)\int_{\theta_1'}^{\theta_1''}[I_s(\theta_1, \theta_x) - I_t]\, d\theta_1$. We reemphasize that this expression is only useful for calculating V at the minima and saddle points, but not elsewhere. To calculate such points as the small oscillations frequencies one must return to (B1).

[1]B. D. Josephson, Phys. Letters 1, 251 (1962).
[2]B. D. Josephson, Advan. Phys. 14, 419 (1965).
[3]P. W. Anderson, *Lectures on the Many-Body Problem*, edited by E. Caianello (Academic, New York, 1964), Vol. 2, p. 113.
[4]P. W. Anderson, in *Progress in Low Temperature Physics*, edited by C. J. Gorter (North-Holland, Amsterdam, 1967), Vol. 5, p. 1.
[5]P. W. Anderson and J. M. Rowell, Phys. Rev. Letters 10, 230 (1963).
[6]J. M. Rowell, Phys. Rev. Letters 11, 200 (1963).
[7]R. C. Jaklevic, J. Lambe, A. H. Silver, and J. E. Mercereau, Phys. Rev. Letters 12, 159 (1964).
[8]R. C. Jaklevic, J. Lambe, J. E. Mercereau, and A. H. Silver, Phys. Rev. 140, A1628 (1965).
[9]J. E. Zimmerman and A. H. Silver, Phys. Rev. 141, 367 (1966).
[10]T. A. Fulton, Solid State Commun. 8, 1357 (1970).
[11]P. W. Anderson and A. H. Dayem, Phys. Rev. Letters 13, 195 (1964).
[12]T. A. Fulton and R. C. Dynes, Phys. Rev. Letters 25, 794 (1970).
[13]R. A. Ferrell and R. E. Prange, Phys. Rev. Letters 10, 479 (1963).
[14]C. Owen and D. J. Scalapino, Phys. Rev. 164, 538 (1967).
[15]A. Th. A. M. De Waele and R. De Bruyn Ouboter, Physica 41, 225 (1969); 42, 626 (1969).
[16]W. C. Stewart, Appl. Phys. Letters 12, 277 (1968).
[17]D. E. McCumber, J. Appl. Phys. 39, 3113 (1968).
[18]J. Clarke, Proc. Roy. Soc. (London) A308, 447 (1969).
[19]J. Swihart, J. Appl. Phys. 32, 461 (1961).
[20]Multiple I_c's in large-inductance double tunnel junction have been observed by previous workers, e.g., J. E. Mercereau, Proceedings of the U. S.-Japan Seminar on Low Temperature Physics, 1967 (unpublished); A. M. Goldman (private communication).
[21]J. Clarke and T. A. Fulton, J. Appl. Phys. 40, 4470 (1969).
[22]These authors have independently suggested the mechanical analog of Sec. III. D. B. Sullivan and J. E. Zimmerman, Am. J. Phys. 39, 1504 (1971).

PHYSICAL REVIEW B VOLUME 6, NUMBER 3 1 AUGUST 1972

Electron Correlations at Metallic Densities. V *

P. Vashishta† and K. S. Singwi‡
Physics Department, Northwestern University, Evanston, Illinois 60201
and Argonne National Laboratory, Argonne, Illinois 60439
(Received 20 December 1971)

In this paper we present a modification of an earlier theory of Singwi *et al.* of electron correlations at metallic densities. The modification consists in allowing for the change of the pair correlation function in an external weak field via the density derivative of the equilibrium pair correlation function. This results in a new expression for the local-field correction. The present theory has the merit of satisfying *almost* exactly the compressibility sum rule and of giving a satisfactory pair correlation function. Results of self-consistent numerical calculations for the static pair correlation function, correlation energy, compressibility, and plasmon dispersion relation for the electron liquid in the metallic-density range are presented. For those interested in the application of the results of the present paper, numerical values of the local-field correction as a function of wave number have been tabulated in the density range $r_s = 1-6$.

I. INTRODUCTION

In a series[1,2] of recent papers Singwi *et al.* have presented a theory of wave-number and frequency-dependent dielectric function $\epsilon(\vec{q}, \omega)$ of an electron liquid in the metallic-density range ($1 \leq r_s \leq 6$). This theory attempts to take into account in an approximate manner both the exchange and Coulomb correlations through a local-field correction (as defined by Nozières and Pines[3]) which depends on the pair correlation function. The latter is related to the imaginary part of the inverse dielectric function through the fluctuation-dissipation theorem. Thus, it is a self-consistent theory. The first version of the theory,[1] hereafter referred to as I, yielded a physically acceptable pair distribution function $g(r)$, but the compressibility sum rule was only poorly satisfied. Although this deficiency was rectified to a considerable extent in a latter version[2] of the theory, hereafter referred to as II, by screening the Coulomb potential entering the local-field correction, the compressibility was not very satisfactory. The theory has since been applied to a variety of calculations[4-7] for free-electron-like metals with a fair degree of success. Results for the generalized paramagnetic susceptibility derived on the basis of this theory have been no less encouraging.[8-10]

Although the local-field correction in the theory of Singwi *et al.* is static, it will in general depend on frequency. The importance of the frequency dependence of the local-field correction in the di-